City-scale potential of geothermal energy in Beijing

By

Jingyi Wan (Pet)

Fourth-year Undergraduate Project

In Group D, 2014/2015

Supervisor: Prof. Kenichi Soga

I hereby declare that, except where specifically indicated, the work submitted herein is my own original work.

City-scale potential of geothermal energy in Beijing

Abstract

To date, fossil fuels have been the sole, largest resources for energy supplies, however, bearing huge environmental concerns. The surging demand for clean, and renewable energy sources have been the centre of research topics for many years. Among which, geothermal energy represents one of the most sustainable and carbon-neutral resources, and has been proved to be viable in numerous applications. The performance of single borehole geothermal technology has been well documented at the city-scale production, backed by data and simulations.

The research is based on analysis of well data in Beijing; with 250 sample points covered about half of all the wells installed in Beijing. Well depth ranges from 250 m to 4090 m. This research aims to develop a city-scale simulation tool for potential usage of deep geothermal energy, by combining the borehole data with geological data and carrying out a Finite Element Analysis (FEA) that studied the pressure and temperature fields.

Field data, and borehole and geophysical data have been backed by statistics. Locations were marked with their latitudes and longitudes. 3D geological map was modelled for Beijing Area, using JewelSuite, which is a full workflow to build complex geological modal, identify the reservoir stratum, and well planning. For detailed influence on pressure of the area due to extraction wells was performed by finite element analysis (FEA), using COMSOL. The fluid and temperature fields were meshed. Extraction rates were inputted into the model to find the equilibrium pressure distribution with calibrated boundary conditions and carefully chosen parameters.

The relationships between the amount of wells and locations, depths of wells and locations were studied. The temperature profile relates linearly with the depths beneath the ground surface. The initial and the gradient of temperature was evaluated and compared with common earth characteristics. The variance of the data at the same depth was estimated to exam the quality of data.

A geological 3D map for the Beijing was constructed with subsurface and mesh grids indicating horizons. Types of soil along depth for each borehole were summarized and

classified. The aquifers, i.e. strata contain hot ground water, were identified. Total number of the stratum based on the classification is 15, amongst them 6 were identified as aquifers.

The 2D simulation for the pressure distribution was carried out. The effects of rock types in the aquifers and the size of boundaries on the pressure distribution were quantified by simulation. Contours of lateral extension for hot ground water to sustain constant extraction rate were identified in 10, 50, 100 and 200 years interval. The area of influence zone was compared with the area of Beijing in order to illustrate the sustainability. The geothermal energy can sustain for 100 years without injection wells before extracting hot water from adjacent cities. This serving time can be largely increased by implementation of injection wells.

With this research results, guideline for geothermal exploration in Beijing was provided. A statistical analysis including distribution of depths of wells and temperatures at the bottoms of wells was carried out. A 3D map that combines the geological information with borehole data was constructed. Horizons and aquifers were identified and meshed in 3D. FEA was employed to simulate the pressure distribution due to extraction wells. Sustainability was illustrated by the influence zone, which is the scale of the region to sustain constant rate of extractions for all wells. The methodology and the simulations tools can be used for other city-scale planning. The 3D geological map can be inputted to numerical tool to quantify the geothermal energy available. 2D FEA is a simplified solution, detailed evaluation required to transfer the thickness data from the geological map in to FEA tool package. The quality of geological model can be improved by either acquiring new geological data or obtaining the seismic and fault data.

City-scale potential of geothermal energy in Beijing

Final Report

Index

1. Introduction 5

1.1. Deep Geothermal Energy 5

1.2. Deep Geothermal Energy in Beijing 6

1.3. Outstanding Issues for Development 8

1.4. 3-D modelling for geothermal energy in City-Scale 8

1.4.1. Estimation of the deep geothermal potential within the Tertiary Limagne basin [13] (French Massif Central) 8

1.4.2. Geothermal Resource Mapping in Northern Switzerland[19] 9

1.5. Main Research Aims 10

2. Statistical and Geological Analysis 12

2.1. Experiment Procedure 12

2.1.1. Statistics Analysis for borehole data 12

2.1.2. Building a 3D Geological Map 12

2.2. Results and Discussions 13

2.2.1. Statistical Analysis 13

2.2.2. 3D Geological Map 20

3. 2D Thermo-Hydro Simulation 24

3.1. Theoretical Basis 24

3.2. Theoretical Basis 24

3.2.1. Governing Equations for Pressure Analysis 24

3.2.2. Transformation for Influence Zone 25

3.2.3. FE Numerical Integration Techniques 25

3.3. Beijing Analysis 26

3.3.1. 2D FE Model 26

3.3.2. Boundary Conditions 27

3.3.3. Parameter Definition 27

3.3.4. Analysis Limitation 28

3.4. Results and Discussions 29

3.4.1. Pressure Distribution 29

3.4.2. Influence Zone 32

4. Conclusion 36

5. Reference 38

Appendix 1 41

Appendix 2-Tables: 42

Appendix 3-Codes: 47

List of Figures

Figure 1 Schematic graphs of the HSA and EGS heat sources [5] 6

Figure 2 Distribution Pattern of China's Geothermal Resources [7] 7

Figure 3 Geological structure in Northern Switzerland with available borehole data and topography 10

Figure 4 Distribution Column Chart for Depth 13

Figure 5 Distribution Column Chart for max. Temperature 14

Figure 6 Example of Interpolation Results of Temperatures along One Borehole 15

Figure 7 Scattered Plot for the Wells Deeper than 1000m 16

Figure 8 Temperature Distribution at 500m Depth 17

Figure 9 Temperature Distribution at 1000m Depth 17

Figure 10 Temperature Distribution at 1500m Depth 18

Figure 11 Temperature Distribution at 2000m Depth 18

Figure 12 Temperature Distribution at 2500m Depth 19

Figure 13 Temperature Distributions along the wells at depth 500,1000,1500,2000,2500,3000,3500 and 4000m 20

Figure 14 Soil Layers along 20 Sample Points 21

Figure 15 3D Geological Map with strata. Permeability is shown. 22

Figure 16 3D model with wells. Available locations and well depths are shown. Transparent Surfaces are Horizons. 22

Figure 17 The Meshed Plan View of Beijing Area with 178 Borehole Locations 26

Figure 18 Pressure Distribution for Typical Gravel 31

Figure 19 Pressure Distribution for Typical Sand 31

Figure 20 Pressure Distribution for Typical Clay 32

Figure 21 Temperature Field at 10 Years 33

Figure 22 Temperature Field at 50 Years 34

Figure 23 Temperature Field at 100 Years 34

Figure 24 Temperature Field at 200 Years 35

Figure 25 Water Contours at Different Time Intervals 35

List of Tables

Table 1 Ranges of Porosities and Permeabilities for Three Typical Soil Types (modified from Bear) 28

Table 2 Peak Pressures with Various Sizes of Boundaries 30

1. Introduction

Geothermal energy has been used commercially for electricity generation since the year of 1913 [1]. In year 2000, the electrical energy generated was 49.2 billion kW h /year, contributing to 0.3% of the world total electrical energy. For some developing countries with low installed electrical power (e.g. in Philippines, El Salvador, and Nicaragua) geothermal energy can be as significant as 20% [2]. With growth in demand as a result of increasing population and increased electrification of the society, alternative energy systems are necessary. Present technology ensures more reliable control over the environmental impact of geothermal energy. By comparing the cost of difference renewable energies, including US $ 2-10 /kW h for geothermal and hydro, US $ 5-13 /kW h for wind, US $ 5-15 /kW h for biomass, and US $ 23-125 /kW h for solar photovoltaic, geothermal stands out to be the least costly method [1]. With the abatement of carbon dioxide emissions, more financial benefits from the carbon taxes are associated. Geothermal energy is commonly divided into shallow systems with depths less than 400 m and deep systems with depths more than 400 m [3].

1.1. Deep Geothermal Energy

Deep geothermal energy is increasingly being explored as an attractive alternative energy source. Conventional shallow hydrothermal resources, such as hot spring, have been effectively exploited in the past century, but their distribution and potential for supplying electricity is limited [4]. Exploration of deep geothermal energy offers new prospects.

The deep geothermal energy can be classified into two categories: Hot Sedimentary Aquifers (HSA) and Enhanced Geothermal System (EGS). EGS creates geothermal resources in hot dry rock through hydraulic simulation. Cold water is pressurized and injected into deep wells, and through a second well hot water is brought back to the surface. Hydraulic simulation needs to pass through the fractured rocks. Hence, the system is referred to as enhanced or engineered [5].

A novel type of geothermal power generation relies on a HSA. The concept of HSA is that he heat resources can be directly extracted without the need of enhancement [5]. The requirements are sufficient water storage within the aquifers and adequate permeability. The major form of heat transfer is heat conduction with the contribution from convection. Unlike EGA, they tend to be located at a shallower depth and are thus cheaper to develop. As shown in Figure 8, the HSA and EGS heat resources are circled. HSA involves the usage of heat energy in the aquifers, mostly for hot water heating application. The layers of rock with hot water resources are aquifers. Soil conditions for HSA systems include: elevated conductive heat flows, typically ranging from 45 to 95 mW/m^2, sufficient volumes of porous and permeable sandstone aquifers at depth and thick overlying sections of clay or coal rich sequences to act as thermal insulation.

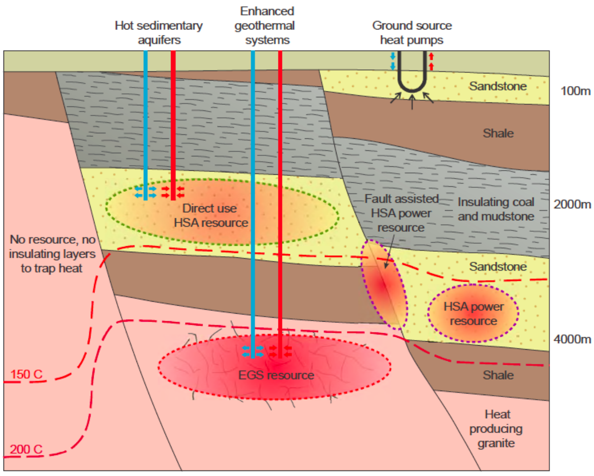

Figure 1 Schematic graphs of the HSA and EGS heat sources [5]

HSA heat plants operate with two-hole systems with injection and extraction wells [6]. The main research focus is on this type of systems. Advantages of an HSA include: (1) relying on natural in situ porosity and permeability, no need for reservoir stimulation, (2) lower technical risk, and (3) lower start-up capital costs.

1.2. Deep Geothermal Energy in Beijing

Geothermal energy represents a far better option, because it can reduce the pressure of energy supply and improving the eco-system. Although there are no natural thermal surface manifestations in Beijing, intensive exploratory efforts have been conducted by Beijing hydro-geologists. City of Beijing is situated on top of a large and deep sedimentary basin where geothermal resources have been found at depth. The location of Beijing with distribution pattern of China's geothermal resources is shown in Figure 2 [7]. Starting from 1970, several hot water resources were discovered at a fairly shallow depth below the city. The total lateral extension of the geothermal field is estimated to be more than 100 km^2 [8].

The Beijing Basin can be divided into ten geothermal areas based on geological and geothermal conditions. The best well-known areas are Urban and Xiaotangshan. These two areas have been utilised since the 70's and 80's. The reservoir rocks in the Urbana and Xiaotangshan systems are limestone and dolomite. The yearly productions of these two areas are about 110 and 120 kg /s, respectively, for each borehole. This results in a water level drawdown of an order of 1.5m /year in the two fields. This indicates that the underlying reservoirs have limited recharge and act as closed hydrological systems. Measures and planning are required to achieve a sustainable usage of the geothermal resources.

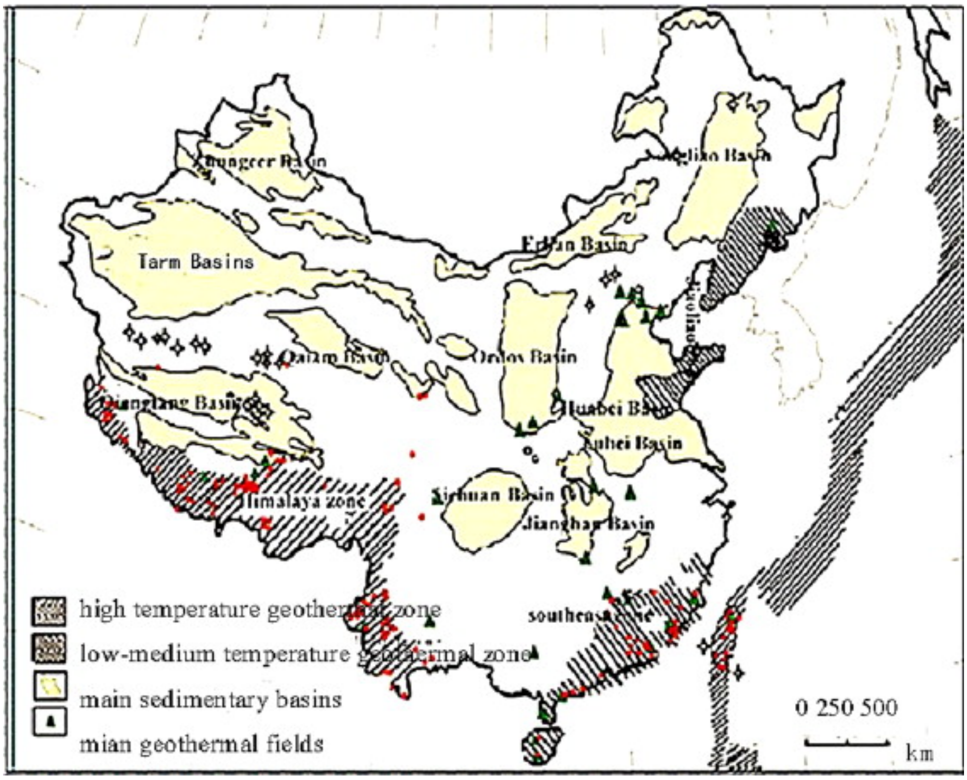

Figure 2 Distribution Pattern of China's Geothermal Resources [7]

One of the Beijing Geothermal fields, Shahe Field, is located at the north part of the city, south to Xiaotangshan field. This field has an area of 100 km^2 [9]. A lumped parameter model has been use to simulate the data collected in that area, the results show an decrease in water level drawn down by the extraction. With reinjection wells, the decrease will be minimized, demonstrating reinjection wells are essential for sustainable utilization of reservoirs [10].

Another important aspect that is critical for sustainable management is the common management of the geothermal resources in Beijing. This is because many different users may be utilising the same reservoir. Adjacent production wells may influence each other. As the resources are limited, the utilisation needs to be carefully planned.

1.3. Outstanding Issues for Development

Number of field data is limited by the borehole samples of the area. The excising borehole amount in Beijing is quite huge with about 600 in total. However, the data are all separated and recorded in separate forms without an integral study. Geothermal reservoirs are generally involved a complex interplay of various petro physical and geological properties. Previous work is more concrete on temperature field with conductive of energy. However, the fluid field and pressure field are critical for the convection. With the development in computer strength for FEA programs like COMSOL, coupling between the pressure and temperature can be performed.

1.4. 3-D modelling for geothermal energy in City-Scale

The usefulness of understanding geology by 3-D modelling is well established [11], [12]. Modelling aims to produce a representation of the real geological condition. This representation can be the ultimate goal of modelling. More often, a 3-D geological model will be inputted to simulation package to quantify its engineering properties. Some examples for such study are given in this Section.

1.4.1. Estimation of the deep geothermal potential within the Tertiary Limagne basin [13] (French Massif Central)

The Limagene basin (Maasif Central, France) is located in a promising zone for geothermal energy, just like Beijing. The major difference is that this basin has never been exploited for its geothermal resources but has been investigated since the 1970s for this purpose. This area is selected due to the following reasons. Most of these grabens have promising geothermal gradients and highly fractured zones in the underlying basement [14], [15]. Many thermal springs occur along the border faults indicating the potential hydrothermal circulation [16]. There was some recent volcanic activity that might represent an additional heat source. Two major aspects are studied in consideration of geothermal exploration.

First, understanding of the geological structure for determining whether the area may host geothermal resources [17], [18]. In order to improve the 3D thermal characterization and estimation of geothermal potential, special attention was paid to the local hydrological regime. The field, borehole and seismic data were interpreted and inputted to form a 3D geological map. The geological model was constructed by the scalar-field interpolation method by 3DGeoModeller software developed by BRGM. The geological layers were then discretized using hexahedra and prisms. Faults were discretized as squares and triangles.

Second, the viability of the geothermal resources was estimated by inferring the available energy. The temperature extrapolated to 5 km depth was modelled and confirmed by a detailed analysis. These and the subsequent subsurface temperature maps were built with linear downward extrapolation. The thermal potential was computed according to (i) the thickness and extent of the aquifer derived from the geological model, (ii) the temperature distribution derived from the numerical model and (iii) the reinjection temperature with heat capacity of the host rock.

This research provided an integrated approach for quantifying the geothermal potential of the region. However, the thermal model assumed that only conduction occurred in the regime. However, the resultant temperature field did not fit the data from boreholes with depth above 1400 m. The fluid circulation occurs and disturbs the local thermal regime, either through water flow within the borehole or through larger-scale fluid circulation. The quality of the geological model would be improved by acquiring new geological data. The geological model can be refined by gravimetric and magnetic data. In conclusion, the 3D geological model, the thermal model and the quantification of the geothermal potential are guideline for the exploration of geothermal resources in the Limagne d'Allier basin.

1.4.2. Geothermal Resource Mapping in Northern Switzerland[19]

A regional evaluation of the potential of geothermal energy was required in Northern Switzerland due to growth in demand in that region. A 3D regional geological and thermal model of 40km extent was built. The subsurface in Northern Switzerland was explored by previous nuclear waste disposal studies. Seismological sections and boreholes were drilled through the sedimentary cove into the crystalline basement. The locations of the various data-bearing boreholes and geological surface structures of two selected units are shown in Figure 3.

After the large-scale structural geological model, the visualized geological layers from the Gocad software [20] was transferred into a numerical scheme. The coupled thermo-hydraulic behaviour was studied by using the FE package FRACTure [21] together with a steady-state, hydraulic Darcy equation. The thermal data basis for the simulation was taken from recent data on Switzerland and neighbouring areas. The temperature data set included borehole bottom hole temperature values and high-resolution temperature logging data. The petro-physical data set included the thermally relevant parameters, i.e. thermal conductivity, porosity, density, heat capacity and hear production.

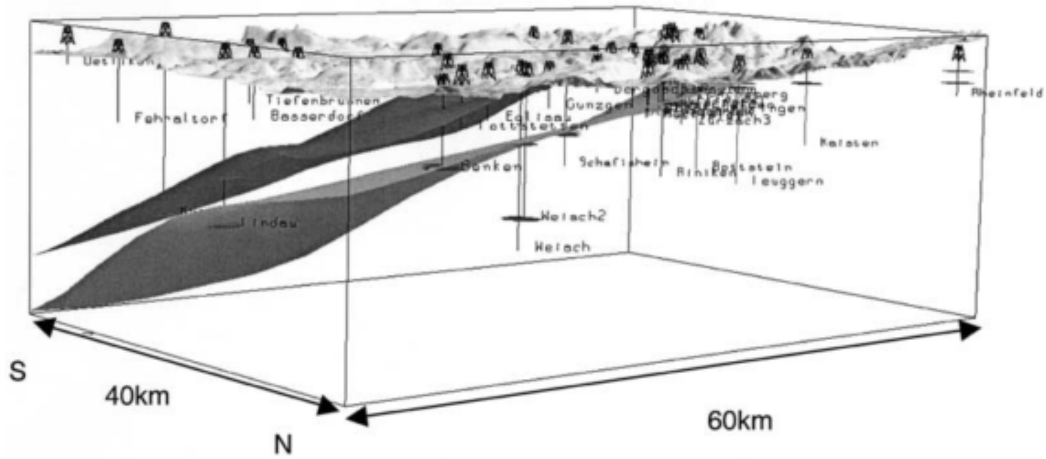

Figure 3 Geological structure in Northern Switzerland with available borehole data and topography

Unlike previous geothermal resource assessments, this full 3D numerical evaluation included geological, hydrogeological and petro physical data. All the parameters were re-assessed by a fully 3D geological and topographical model. Temperature field was evaluated by solving energy equations. However, too few boreholes were available to obtain a complete investigation of the area. Also the recovery factors for the temperature field were based on numerous assumptions. Further operational data is required to validate the assumptions.

1.5. Main Research Aims

This research aims to develop a city-scale simulation tool for potential usage of deep geothermal energy in Beijing. This tool can build the confidence for the large-scale applications of geothermal systems with particular geological conditions. This tool should be able to obtain the subsurface temperature, to predict the life span of the geothermal system for a given abstraction rate, and to suggest a proper abstraction for the sustainability of the deep geothermal system. My main focus is to design, validate and modify the simulation tool based on data from Beijing. The data are from reliable sources including Tsinghua University and the Ministry of Land and Resources of China. The data cover about half of all the existing boreholes in Beijing and hence this research should have sufficient data to produce a representative and reliable result. The research is divided into three parts:

- Statistical analysis for the relationship between well locations, temperature profile and depth along wells
- Building a geological map with borehole data
- Building coupled thermal-hydro mechanical interactions for the injection and extraction wells. Producing an influence zone for study of sustainability.

2. Statistical and Geological Analysis

2.1. Experiment Procedure

2.1.1. Statistics Analysis for borehole data

The borehole data used in this study are in separate forms. All the location data were recorded as the addresses of boreholes. The addresses were transferred into geographic coordinate system with latitudes and longitudes, which were found from Google Map. Data were collected in the year from 1970 to 2000. Due to this long span of time, some addresses have changed names, thus cannot be transferred into geographic coordinates.

Excel was used to produce one form that summarizes all the well locations with temperatures along each well.

Temperatures along wells have very different mean values and ranges. Interpolation method was required in order to find temperatures at the same depths. As depth ranging from 100 m to 4000 m, the 4000 m length was divided into 40 groups, each with an interval of 100 m. This is done in Matlab. The Matlab code for interpolation is in code 1 in the Appendix 3. The linear assumption would be appropriate as the temperature reaches an equilibrium state with some stationary diffusion coefficient. After interpolation, temperatures distribution graph at the same depth was plotted for different depths by using excel. Temperatures were plotted in the same graph, and compared with theoretical temperature along depth. Outliers were identified. The amount of outliers can be used to show the quality of the data. This was done in a Matlab code given as code 2 in Appendix 3.

2.1.2. Building a 3D Geological Map

As research focussed on the analysis based in Beijing, a geological model was produced. A professional program JewelSuite, developed by Baker Hughes, was chosen, as it is a full workflow integration program to build complex reservoir models. The functions most relevant to the research are structural modelling and well planning. The first step was to input the wells locations with their depths into the program. The second step was to input the petro-physical properties and geological properties into the model. The soil types were classified into three main groups: sand/ quartz/ conglomerate, mudstone/ slate/ tuff, dolomite/ limestone. The classification was based on the porosity and permeability of these three types of soil. Layers containing sand/ quartz/ conglomerate were identified as aquifers where hot ground water locates and is suitable for extraction. 16 borehole data were selected and interpolated over the whole Beijing area. These borehole data were chosen to be representative points due to their sufficient depth and good quality of soils identification along the depth. With the locations and types of soils for 16 samples, polylines connecting between points were produced, and inputted into the polyline set area in order to generate the geological surface of horizons and strata of aquifers.

2.2. Results and Discussions

2.2.1. Statistical Analysis

2.2.1.1. Overview of Borehole Data

A short summary of the initial data is given here. There are 247 wells in total. As already specified, the samples cover nearly half of all the wells in Beijing. The results should be representative. Amongst these 247 borehole data, 183 borehole data is useful due to the fact that the other boreholes' addresses no long exist. The extreme data are listed below for both depths and temperatures. The maximum and minimum depths are 4088.88 m and 250 m respectively. The maximum and minimum temperatures are 91.9 °C and 25.12 °C respectively. The distribution in percentage of the depth and temperature are summarised into two pie charts (shown in Figure 4 and Figure 5 below).

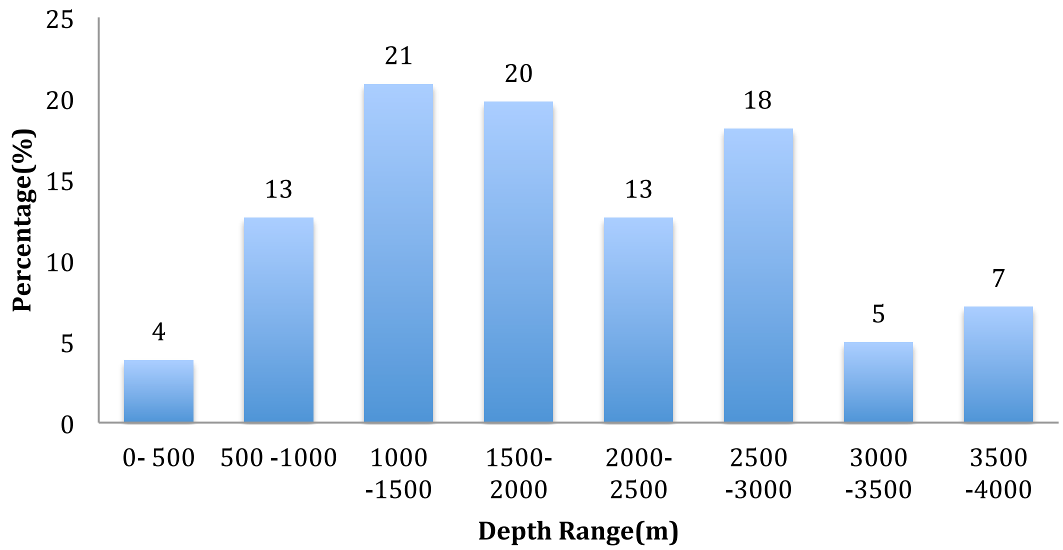

Figure 4 Distribution Column Chart for Depth

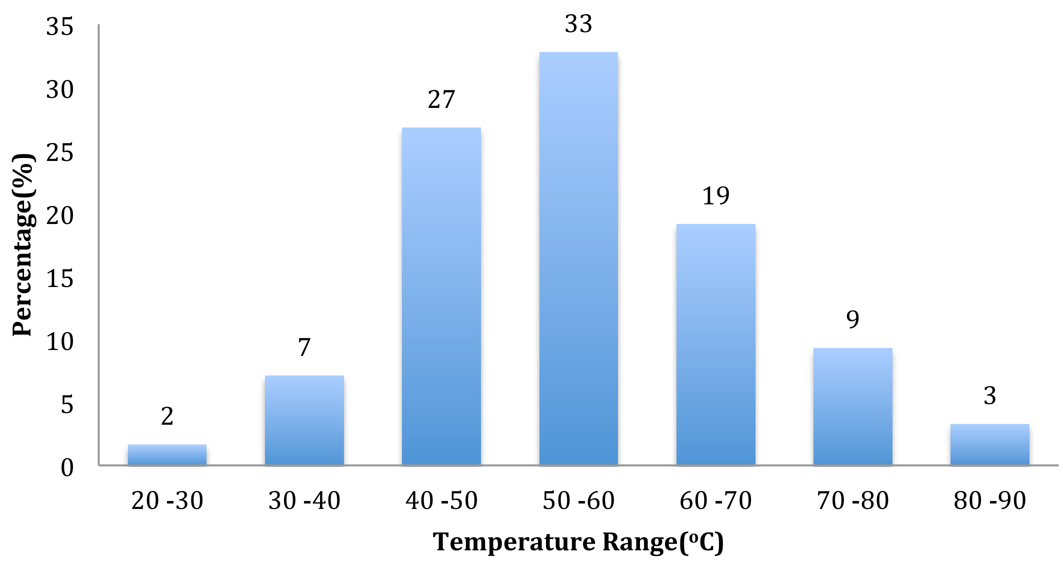

Figure 5 Distribution Column Chart for max. Temperature

Looking into the first depth column chart, depths ranging from 1000 m to 2000 m are the major well depth, with 40% in total. Depths that range from 2000 m to 3000 m have significant percentage as well, with 31% in total. Only a small proportion of wells are either shallower than 1000 m or deeper than 3000 m. Thus, the analysis for the temperature field at depth ranges from 2000 m to 3000 m is more reliable, as there are more sample points located in these depths.

As for the temperature distribution, its majority is between 40 °C and 60 °C comprising 60% in total. Temperature ranges from 60 °C to 70 °C is considerably significant with 19%. A considerably smaller number is higher than 80 °C. The results show that the well temperatures are not as high as expected. The reason might be that the wells currently examined are not deep enough. Interpolation methods should be used to find temperatures at deeper locations, say from 3000 m to 5000 m.

2.2.1.2. Interpolation of Temperatures along Depths

By using the code in Matlab, the temperatures at every 100 m intervals were interpolated and summarized into an excel form. One example graphic result of the interpolated temperatures along one borehole is shown in Figure 6. As shown on the graph, original data are shown as blue crosses, and fitted data are shown as red circles. The linear assumption would be appropriate as the temperature reaches an equilibrium state with some stationary diffusion coefficient. Reliability of the interpolation results depends on the quality of the original borehole data. If the temperatures along the depth are recorded in approximately similar intervals and the range of depths is wider, say longer than 1000 m, the interpolated results would be more reliable.

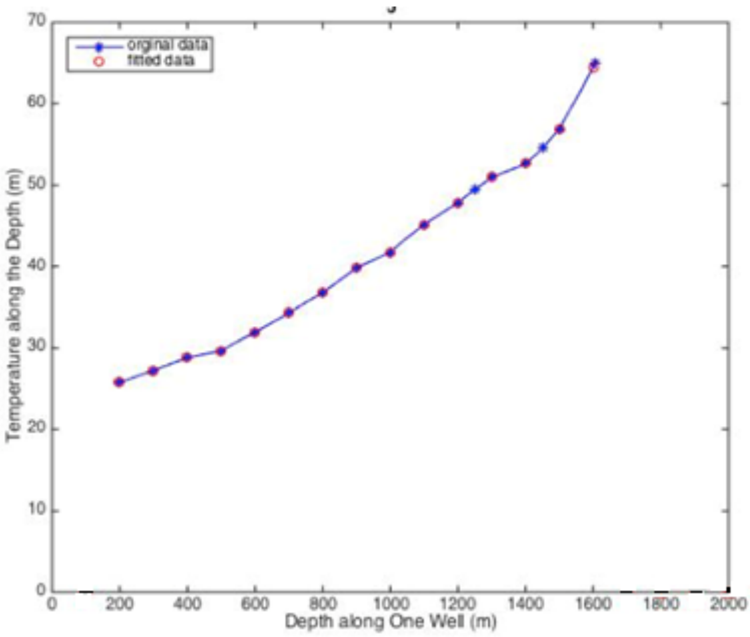

Figure 6 Example of Interpolation Results of Temperatures along One Borehole

2.2.1.3. Locations of Wells

Firstly, the relationship between number of wells and locations was studied. The scattered points for wells with depths larger than 1000 m are shown in Figure 7. Wells less than 1000 m are too shallow for potential use as deep geothermal extraction wells.

The geographic coordinate system with latitudes and longitudes are used from x-axis and y-axis. This coordinate systems can be transformed into standard length unit km conviniently by employing following equations, in order to further investigate the geothermal potential.^{o}c

$$\text{Longitude: } 1^{o} = 111km$$
$$\text{Latitude: } 1^{o} = 111km \times cos(latitude)$$

From the scattered plot, most of wells located in the range from 116.1^{o} to 116.6^{o} in longitude, and 40.2^{o} to 39.7^{o} in latitude (as shown by the red rectangle). The reason for this concentration of distribution might be due to the extent of development in the area. In urban area (i.e. close to the city centre), more boreholes are drilled to study the underground behaviour. This result shows that the analysis of the temperature field is more reliable in the central region of Beijing, compare to the outer area where less boreholes were drilled and analysed.

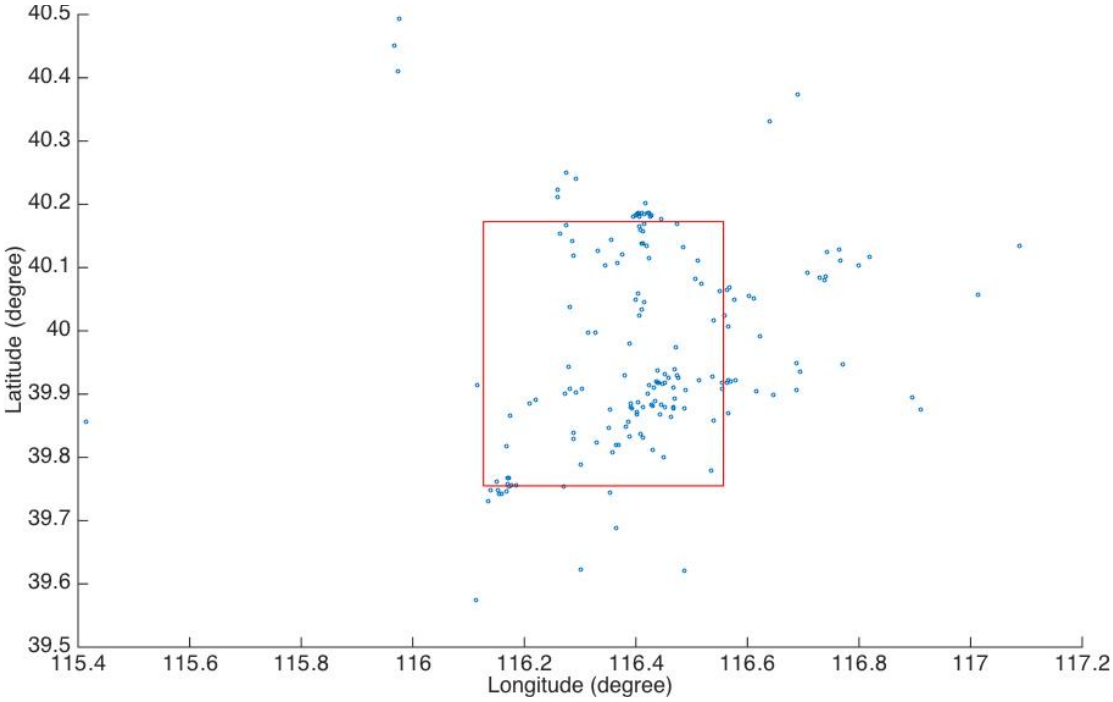

Figure 7 Scattered Plot for the Wells Deeper than 1000m

2.2.1.4. Temperature Profile along the well

The amount of temperature data available for 500 m, 1000 m, 1500 m, 2000 m, 2500 m, 3000 m, 3500 m and 4000 m are 130, 131, 102, 74, 54, 24, 15 and 2, respectively. The average temperatures are 32 ^{o}C, 40 ^{o}C, 45 ^{o}C, 50 ^{o}C, 57 ^{o}C, 62 ^{o}C and 66 ^{o}C, respectively. The amount of data higher than 2500 m is not sufficient to support a reliable analysis.

The distribution graphs for depths at 500 m, 1000 m, 1500 m, 2000 m and 2500 m are shown in Figure 8~Figure 12. The heights of the columns in the graphs present the percentage of temperature lying in each interval.

For 500 m depth, as shown in

Figure 8, the most frequent temperature interval is 30~40 ^{o}C (52%), with 37% lower than 30 ^{o}C and 13% higher than 40 ^{o}C. The minimum and maximum temperatures are 14 ^{o}C and 53 ^{o}C, with a difference of 39 ^{o}C. The average at this depth is 32 ^{o}C.

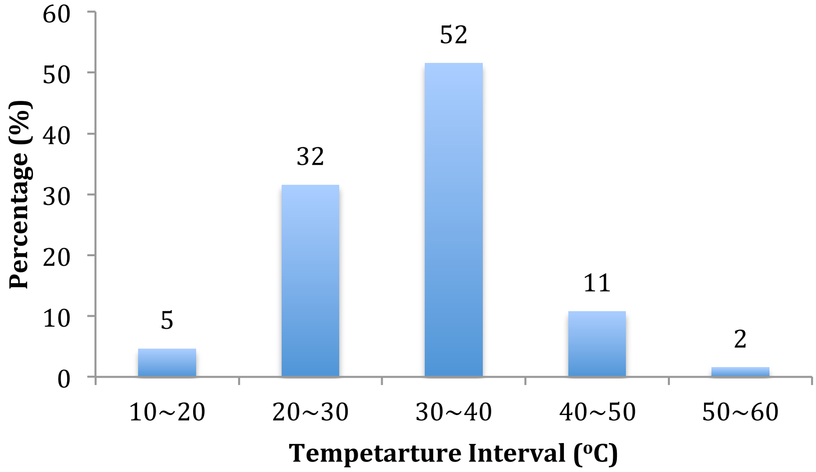

Figure 8 Temperature Distribution at 500m Depth

For 1000 m depth, as shown in Figure 9, the most frequent temperature intervals are 30~40 °C (39%) and 40~50 °C (36%), with 13% lower than 30 °C and 12% higher than 50 °C. The minimum and maximum temperatures are 16 °C and 59 °C, with a difference of 43 °C. The average at this depth is 40 °C.

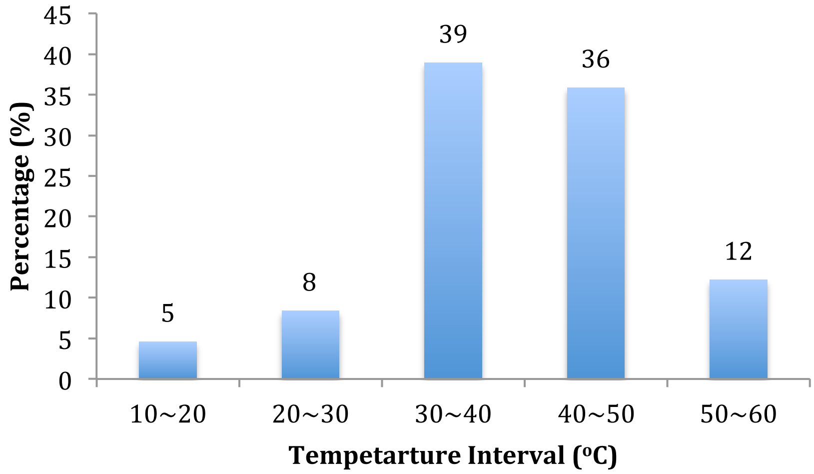

Figure 9 Temperature Distribution at 1000m Depth

For 1500 m depth, as shown in Figure 10, the most frequent temperature interval is 40~50 °C (42%) with 23% lower than 40 °C and 35% higher than 50 °C. The minimum and maximum temperatures are 17 °C and 67 °C, with a difference of 50 °C. The average at this depth is 45 °C.

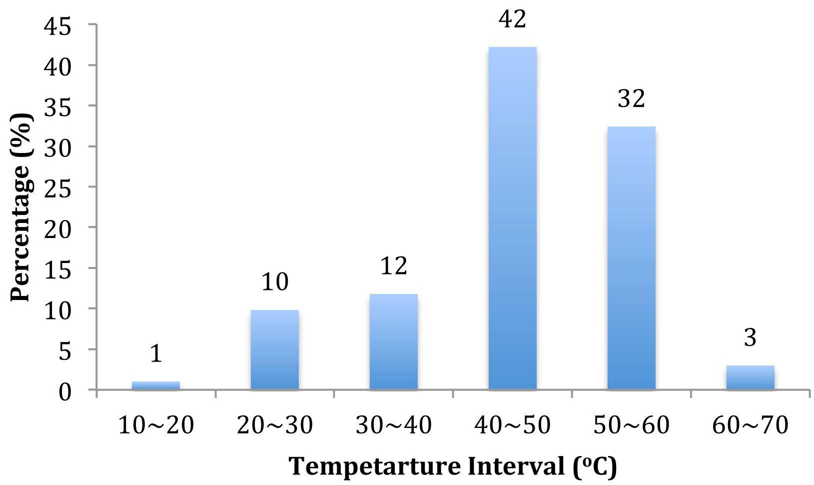

Figure 10 Temperature Distribution at 1500m Depth

For 2000m depth, as shown in Figure 11, the most frequent temperature interval is 50~60 °C (34%) with 46% lower than 50 °C and 20% higher than 60 °C. The minimum and maximum temperatures are 21 °C and 76 °C, with a difference of 54 °C. The average at this depth is 50 °C.

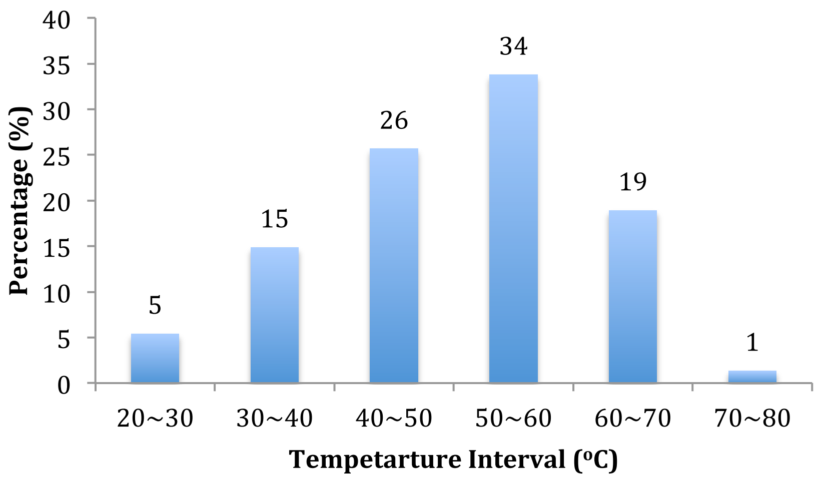

Figure 11 Temperature Distribution at 2000m Depth

For 2500 m depth, as shown in Figure 12, the most frequent temperature interval is 60~70 °C (35%) with 52% lower than 60 °C and 13% higher than 70%. The minimum and maximum temperatures are 21 °C and 76 °C, with a difference of 54 °C. The average at this depth is 57 °C.

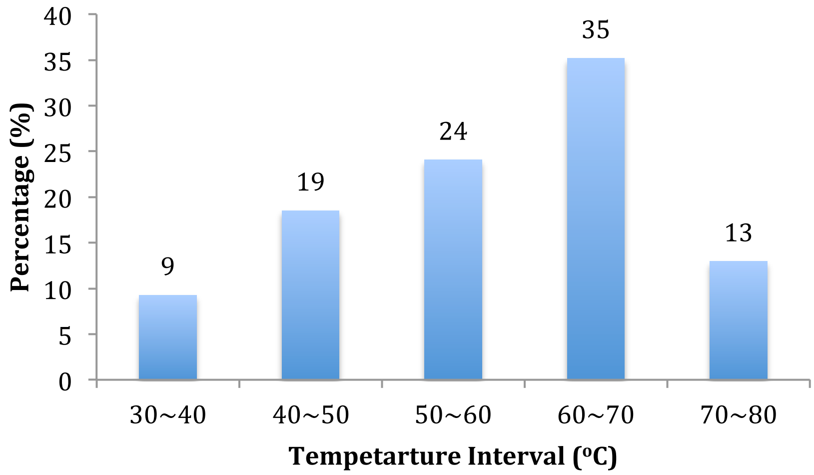

Figure 12 Temperature Distribution at 2500m Depth

The average temperatures for each depth lie within these peak interval, which indicates that the mean and medium value is quite close and the data set is not too skewed. The average temperatures increase continuously about 6 °C each 500 m. The temperature varies a lot for each depth, with about 50 °C for extreme values. However, the variation for the most temperatures in same depth is about 10 to 20 °C. Hence, if we exclude the outliers, then the result is quite consistent.

After the analysis for the temperature distribution for each depth, a combined graphic result is shown in Figure 13. The blue dots represents the temperature logs along the depths and there is a clearly increase in temperature along the depths. The temperatures from 500 m to 1500 m show a concentration at middle temperatures, which indicated the variances at these depths are small, and the mean values lie in the confident interval. However, the blue dots at depths from 2000 to 4000 m are quite separated, partly due to the fact that the temperature logs at these depths are less than those at shallower depths. This indicated that the mean value might not be representative for the temperature at deep locations. The red solid line is the theoretical gradient for the temperature profile, as shown in the following equation:

$$T = 15 + 30/1000H$$

where T is the temperature along depth and H is the depth beneath the ground level.

The ground level temperature is assumed to be 15 °C, by averaging the annual temperature variance in Beijing. The gradient in this equation, 30/ 1000, reflects that the temperature increases 30 °C per kilometre as the depth from earth surface to interior [2].

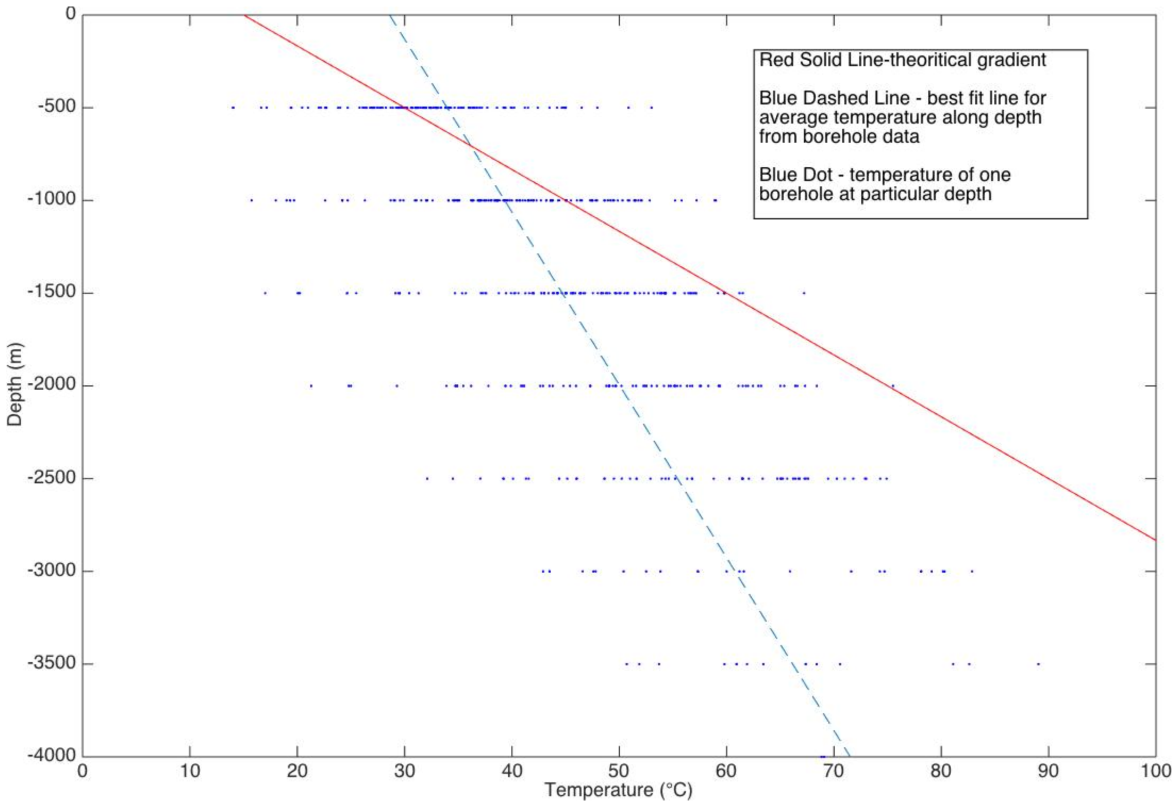

Figure 13 Temperature Distributions along the wells at depth 500,1000,1500,2000,2500,3000,3500 and 4000m

The dashed blue line indicates the best-fit line for the average temperatures along the depths of boreholes. The equation for the best-fit line is shown as following:

$$T = 28.6 + 10.7/1000H$$

This indicates that the average ground temperature is 28.6 °C, which lies within the ground temperature ranging from 16.4 °C to 40.5 °C, with a mean of 26.6 °C, reported by Xiao, R B and co-workers [22]. The gradient of this equation, 10.7/ 1000, indicates that the temperature increases 10.7 °C per kilometre as depth increases. This is lower than the gradient in the previous equation. This might due to the fact that the local geothermal energy has been extracted for more than 40 years, which causes a decrease in ground temperature. Another possible explanation might be that Beijing locates in ancient continental crust, and the gradient for this type of crust can be as low as 10 °C/ km [2].

2.2.2. 3D Geological Map

The rock types for 20 sample points are shown in Figure 14. There are 14 strata in total, where amongst them, 6 strata are identified as aquifers. The average depths for these 6 aquifers are 240.8 m, 870.9 m, 1285.3 m, 1730.9 m, 2137.5 m, and 3684.7 m. The average thickness of these aquifers from shallowest to deepest are 240.8 m, 239.4 m, 84.0 m, 182.3 m, 179.6 m, and 560.7 m.

Then these sample points were inputted into JewelSuite. As shown in Figure 15, the horizons and strata with colours indicate whether the stratum is aquifer or not. The strata displayed in blue are aquifers, and the strata displayed in tan are non-permeable layers. The sub-surfaces of the horizons were fully interpolated by meshing with triangulated areas, and linear relationship between adjacent nodes. In this model, geological layer thickness is controlled by data location. The model enables positions of the geological formations at any point in the 3D space within Beijing. The geological layers are discretized using hexahedra and prisms.

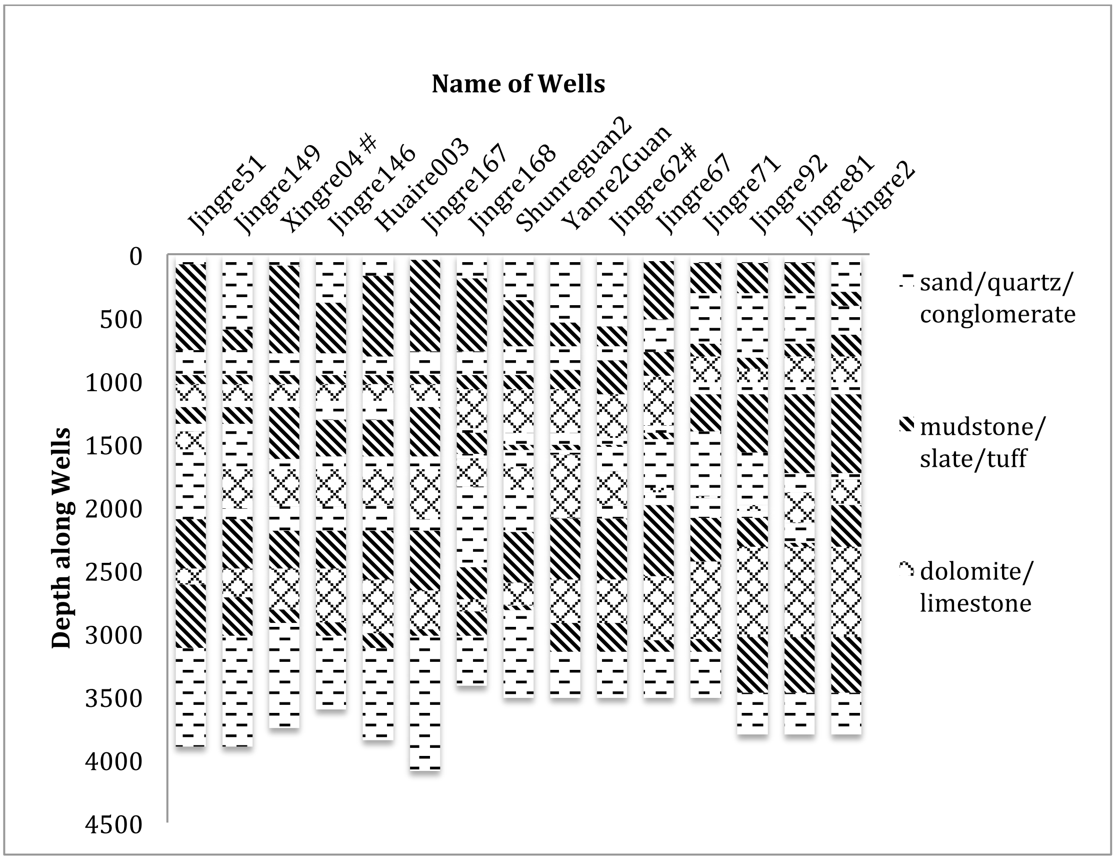

Figure 14 Soil Layers along 20 Sample Points

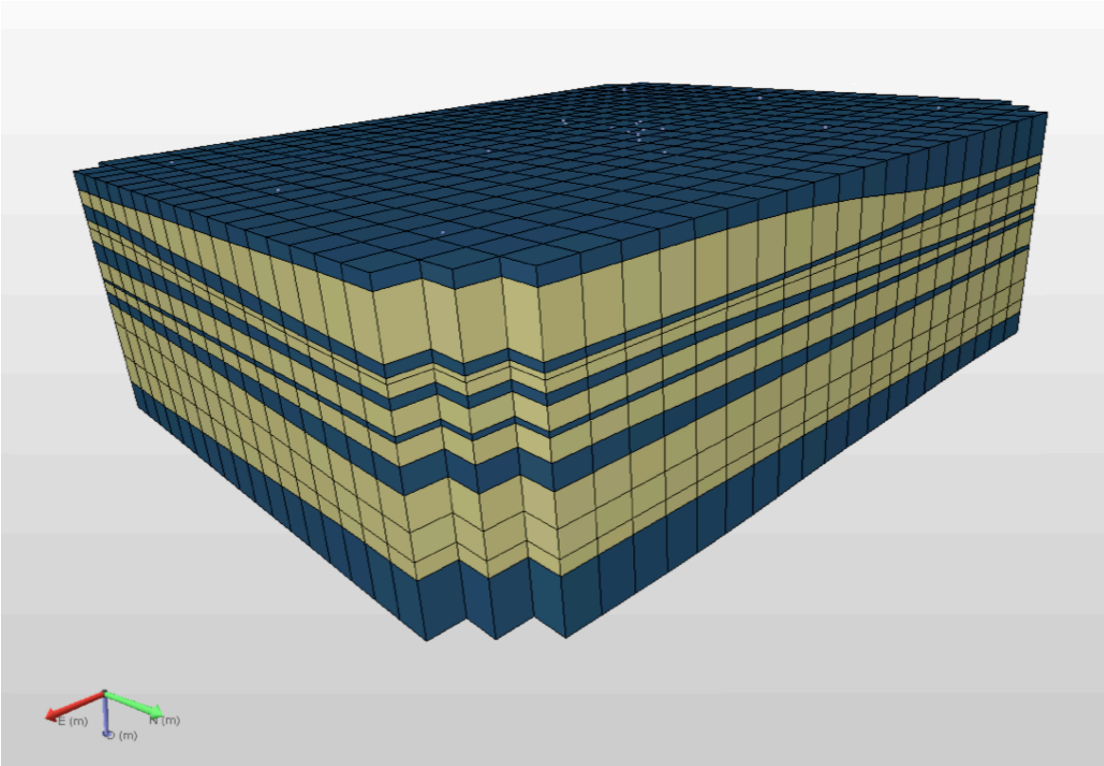

Figure 15 3D Geological Map with strata. Permeability is shown.

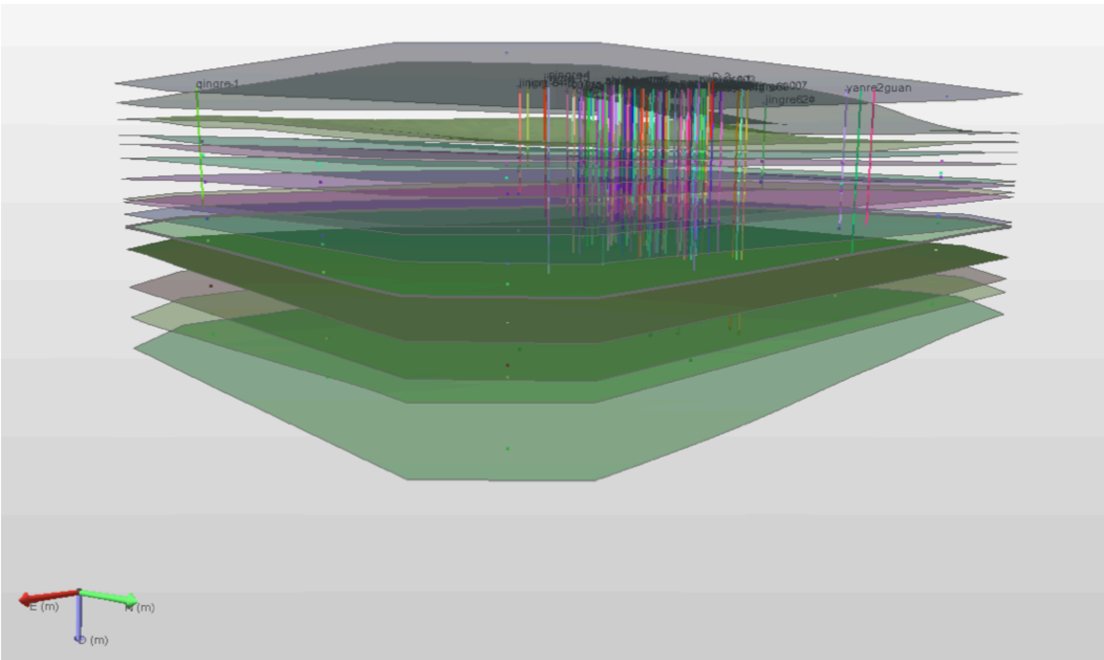

Figure 16 3D model with wells. Available locations and well depths are shown. Transparent Surfaces are Horizons.

The locations of various data-bearing boreholes are illustrated in Figure 16. The length of the well refers to the depth of the well beneath surface. Transparent surfaces are horizons identified previously. After identifications of aquifers, the wells locate in each aquifer can be found.

The large-scale structural geological model can be transfer into other numerical scheme with output files. This methodology allows us to construct the geological map with limited sample points. Visualised the horizons with aquifers and well locations. The quality of the geological model would be improved by acquiring faults data, seismic data and more accurate field test with properties of rock including porosity, permeability and thermal conductivity.

3. 2D Thermo-Hydro Simulation

3.1. Theoretical Basis

Rock is a multi-phase medium (particles and water), hence requiring a complex analysis involving a fixed matrix and a floating liquid. Specialised Finite Element (FE) software is required to simulate the multi-physical material. COMSOL was used for the analysis, as a suite of multiphase simulation platform is in-built to couple the multi-phase medium with coupling effects. Furthermore, COMSOL includes the graphical user interface (GUI) and a set of predefined user interfaces which many the manipulation of the program self-explanatory and easily understandable. COMSOL is also widely used in academic and industrial finite element analysis (FEA) in interfaces for electrical, mechanical, fluid flow and chemical applications. Therefore, results from the program can be interpreted and transferred for future improvements easily.

3.2. Theoretical Basis

3.2.1. Governing Equations for Pressure Analysis

COMSOL has in-built equations for relationship between extraction pressure and extraction fluid rate in the pore fluid, which relies on Darcy's Law.

Darcy's Law

$$\dot{m} = \nabla \cdot (\rho q)$$

$$q = -\frac{\kappa}{\mu}\nabla p$$

where

$\dot{m}$ is mass flow rate, kg/s;

ρ is mass density of the fluid, kg/m^3;

q is discharge rate per unite area, m/s;

κ is intrinsic permeability of the medium, m^2;

μ is viscosity, Pa·s

The sustainability of the geothermal energy in Beijing is studied according to the influence zones at different time periods. The influencing contours are the region where the hot ground water is exhausted at particular moment.

3.2.2. Transformation for Influence Zone

The process of extraction and injection is reversible. Therefore, the contours of water during extraction are the same as the contours during injection. The contours of water can be exactly the same as the contours of temperature if the parameters of the model are carefully chosen. The fluid velocity in the rock and heat flow velocity can be derived from Darcy velocity. The properties of the medium can be derived from the properties of the fluid and solid. Equations are as shown in below.

$$u = q/n$$

where
u is fluid velocity, m/s
q is Darcy velocity, m/s
n is porosity
v is heat flow velocity, m/s
ρ is density of medium
c is heat capacity of medium
ρ_f is density of fluid
c_f is heat capacity of fluid
ρ_s is density of solid
c_s is heat capacity of solid

By equating the fluid and heat flow velocity, the water field is the same as the temperature field if heat capacity of solid (matrix in the model) is zero. The thermal conductivity of fluid is set as fluid is modelled as temperature.

3.2.3. FE Numerical Integration Techniques

For this particular problem, the analysis was stationary, and was performed using finite element method. The domain was divided into triangulated elements with controlled size. Then the differential equation was integrated over the elements meshed by COMSOL. The result is a set of linear algebraic equation, one for each element. The elemental value was solved iteratively until it reaches to a convergent solution.

3.3. Beijing Analysis

3.3.1. 2D FE Model

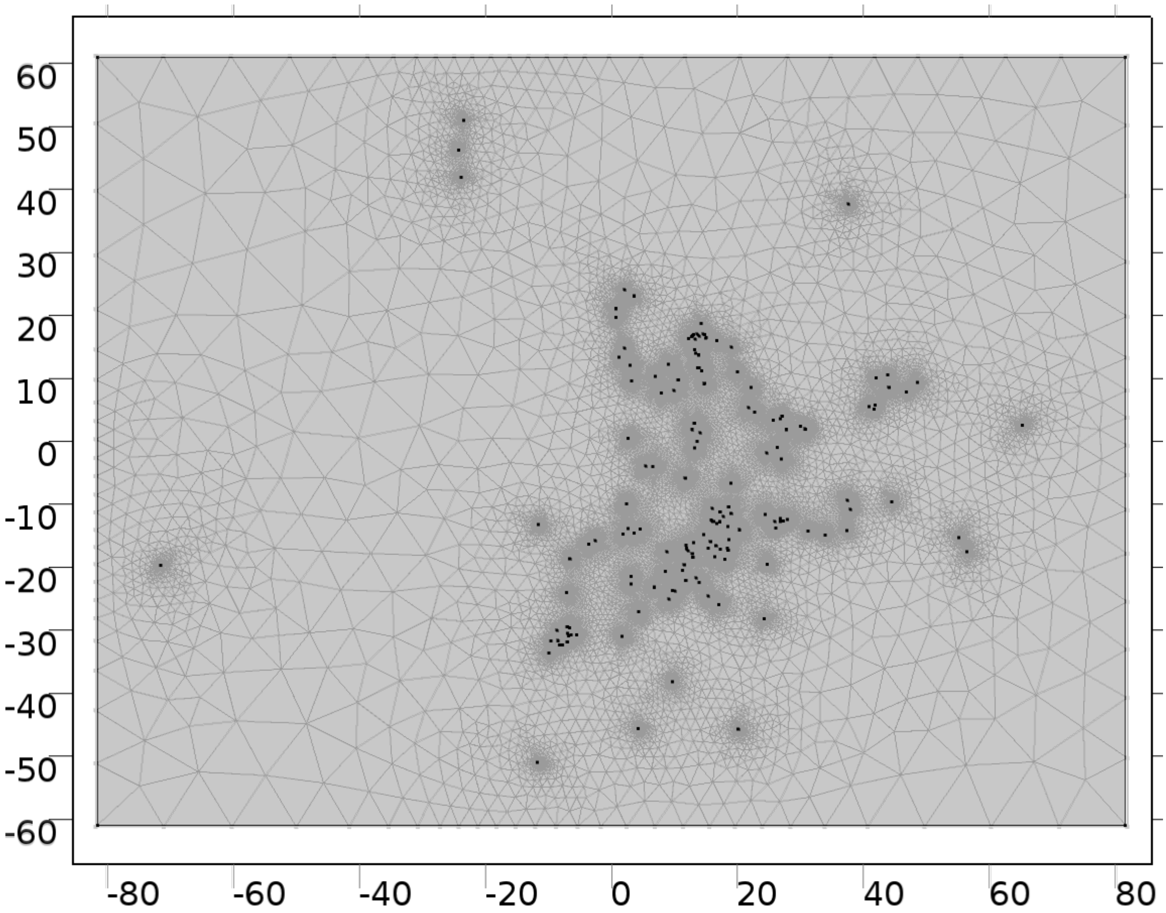

Figure 17 The Meshed Plan View of Beijing Area with 178 Borehole Locations

The analysing region in Beijing has a lateral extension of 143km×102km. This is determined by the furthest boreholes locations. 178 wells, with reasonable quality of outflow rate from the bottoms of the wells, locate in this area. The radiuses of these wells are assumed to be 5m, which is much higher than the actual radius. However, as pressure is only relevant to volumetric flow rate, the increase in radius is acceptable, and makes the FEA computation faster.

The mesh is composed of non-uniform triangular elements, with solid points representing well locations, as shown in Figure 17. The mesh is finer closer to the wells, which is where most flow concentrations, and higher-pressure gradients are expected to occur. The model is a 2D model that simplified from 3D problem. Therefore, the model thickness is assumed to be uniform and has a value of 1m. The computed extraction rate will be per unit metre thickness.

3.3.2. Boundary Conditions

For pressure distribution simulation, the boundary of the analysed region is assumed as a zero-pressure boundary. The boundaries are assumed to be 10km larger each side in both x-axis and y-axis.

The outflow velocity extracted from each well is calculated from the extraction rate, as shown in following equations. The extraction rates are recorded in the borehole measurement data. All volumetric rates are outlet boundary conditions.

$$A = 2\pi r l$$

$$v = \frac{Q}{A \times 3600 \times 24}$$

where
A is area of the well, m^2;
r is radius of the well, 5m;
v is outlet velocity, m/s;
l is the aquifer thickness
Q is volumetric extraction rate, m^3/day.

The borehole extraction rates Q and the calculated outlet velocities v for all wells are tabulated in Appendix 2.

As the influence zone is model in thermal field, the injection fluid temperature is 20 ^oC, and the initial hot water in the aquifer is 70 ^oC. The border for temperature field is sized as 200 km by 200 km, which is larger than the pressure distribution boundary in order take into account of the rural area in Beijing.

3.3.3. Parameter Definition

The rock formation is assumed to be fully saturated. The two phases in the aquifers are permeable rock and water. Two parameters involved in the Darcy's equation for fixed matrix are porosity and permeability. Porosities and permeabilities of three typical rock types are shown in Table 1. The aquifers contain typical rock with porosity equals to 0.36 and permeability equals to $10^{-9}cm^2$.

	Porosity	Permeability (cm^2)
Unsorted Gravel	0.2	10^{-6}
Typical sandstone	0.36	10^{-9}
Typical claystone	0.51	10^{-12}

Table 1 Ranges of Porosities and Permeabilities for Three Typical Soil Types (modified from Bear)

3.3.4. Analysis Limitation

The extraction pressures analysis is subjected to numerous limitations, due to need of simplification, limited computational accuracy and boreholes data. The simulation in the city-scale serves as a guideline for overall planning in the whole, while for detailed borehole extraction pressure and fluid, this result is quite crude and can be only used as estimation.

- Geometry Simplification

The 3D geological map is simplified into 2D simulation. The aquifers analysed are the shallow aquifers at a depth of 0.5~1km. Therefore, it is acceptable to assume that most of boreholes would be feasible for extraction of hot water from this aquifer. The process to convert the 3D problem to 2D is to assume the aquifer layer is uniform with a constant thickness. The running of analysis in 3D would require a more accurate data set for aquifer thickness. The wells that can extract water from a particular aquifer need to be identified.

The effect of the ground water extraction is assumed to be limited within a finite region. In practice, there is no clear zero-effect boundary.

- Formation Simplification

The porosity and permeability of aquifers is selected as constant values for typical sandstone. However, the porosity and permeability are affected by the confining stress and consolidation of the soil. The porosity and permeability might change a lot with different depth and different geographical coordinates.

The rock is model as an isotropic material with same porosity in all directions. However, the rock might be anisotropic due to the shapes of the grain particles. For instant, plate-shaped particles are very permeable with water flow parallel to plate direction, while very impermeable with water flow perpendicular to the plate direction.

- COMSOL Numerical Accuracy

COMSOL has finite numerical accuracy. By using smaller size meshes and higher order shape functions, the accuracy can be improved. However, both methods will cause a higher computational cost.

COMSOL runs by performing iteration methods. This introduces inaccuracies, as a tolerance error is allowed in each step. By decreasing this tolerance, the accuracy can be further improved. However, this might increase the risk that results is not a convergent solution.

3.4. Results and Discussions

The results of 2D analysis are displayed in two sections: pressure distribution and influence zone due to ground water extraction. There is no change in temperature field due to the fact that there are no injection wells; the only change is the quantity of hot water resources available. The temperature is constant over the analysing period, here the temperature is assumed to be 40 ^{o}C, which is the average temperature at 1000 m as mentioned before. This aquifer refers to the second aquifer from ground surface based on the geological model derived from the borehole data. The average thickness for this layer is 239.4 m based on the strata dividend in section 2.2.2.

3.4.1. Pressure Distribution

The pressure distribution was analysed with the change in rock types and change in zero-pressure boundary. Typical soil types and properties of interests are summarised above.

Keeping the zero-pressure boundary to be 10 km away from the furthest boreholes, the pressure change distributions were interpolated for different permeability values, with surface plots and contour plots, as shown in Figure 18, Figure 19, and Figure 20, respectively. The x-axis and y-axis are the relative position in kilometre. The surface legend is shown on the right of the graph. Red region is zero- pressure zone, indicating zero influence on pressure. Blue region is where the pressure needs to be reduced most in order to extract the hot water out under equilibrium state with constant extraction rates, indicating the most influence zone.

The graphic outputs show clearly a similar tends with a gradually attenuating impact on pressure from centre to the boundary. The most influence zone is located in at about 15km and -10km in x-axis and y-axis. The region of influence zone with nearly 80% of peak pressure is from 0 to 30km in x-axis and -25km to 20km in y-axis, which is about 7% of the overall area of analysis.

Major differences with different rock types are the magnitudes of pressure reduction to pump out same amount of ground water. Peak pressure reductions in gravel, sandstone and claystone are 68.9 Pa, 6.89×10^4 Pa, and 6.89×10^7 Pa respectively. The decreases in pressures are mainly caused by the differences in permeability. There is a clearly an inversely proportional relationship between magnitude of pressure and permeability, i.e. the higher the permeability, the lower in reduction in pressure, as the permeability is measure of easiness of mobilization of fluid in the medium. The reduction pressure in sandstone and gravel is less than 1 atm, which is achievable pressure using pumping system, while the reduction pressure in clay is about 1000 atm, which is not feasible to pump out water.

The materials in one aquifer are not likely to be a single type of rock in realistic. Possible changing of properties and hence the pressure reduction due to combination of different soils should be further assessed.

Distance from furthest boreholes (km)	10	20	30	40
The peak pressure (10^4Pa)	6.89	7.51	8.11	8.62
Increase in Peak Pressure (10^4Pa)		0.62	0.60	0.51
Percentage of Increase in Pressure (%)		9.00	7.99	6.29

Table 2 Peak Pressures with Various Sizes of Boundaries

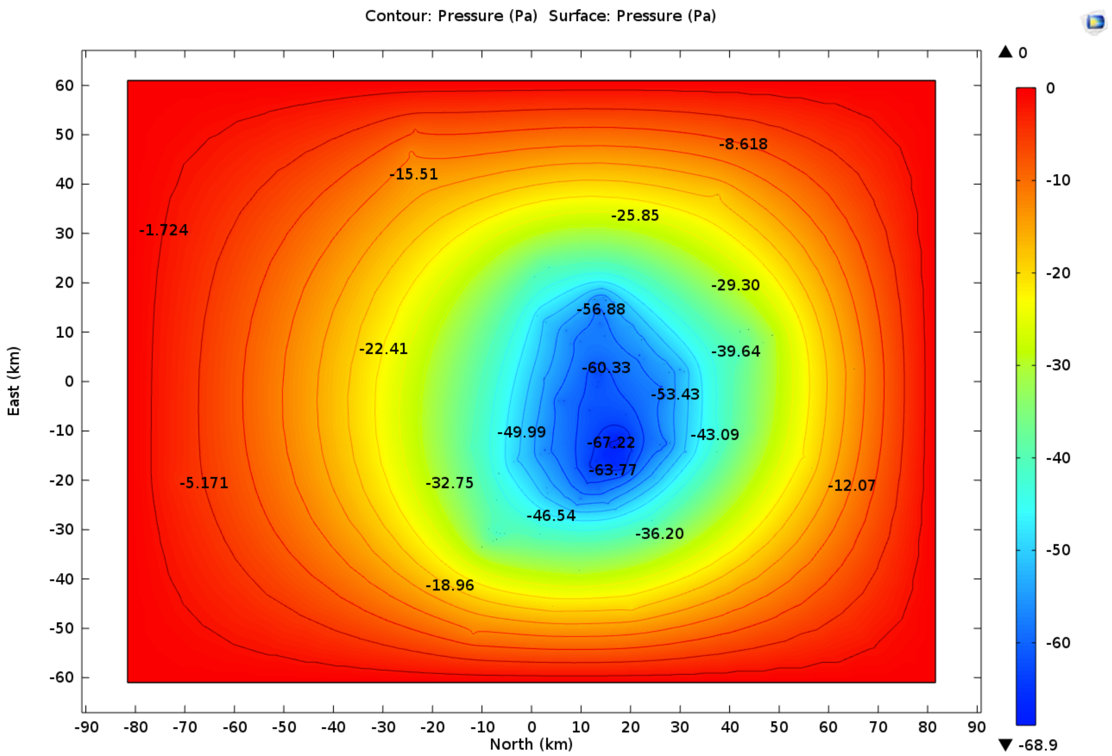

Figure 18 Pressure Distribution for Typical Gravel

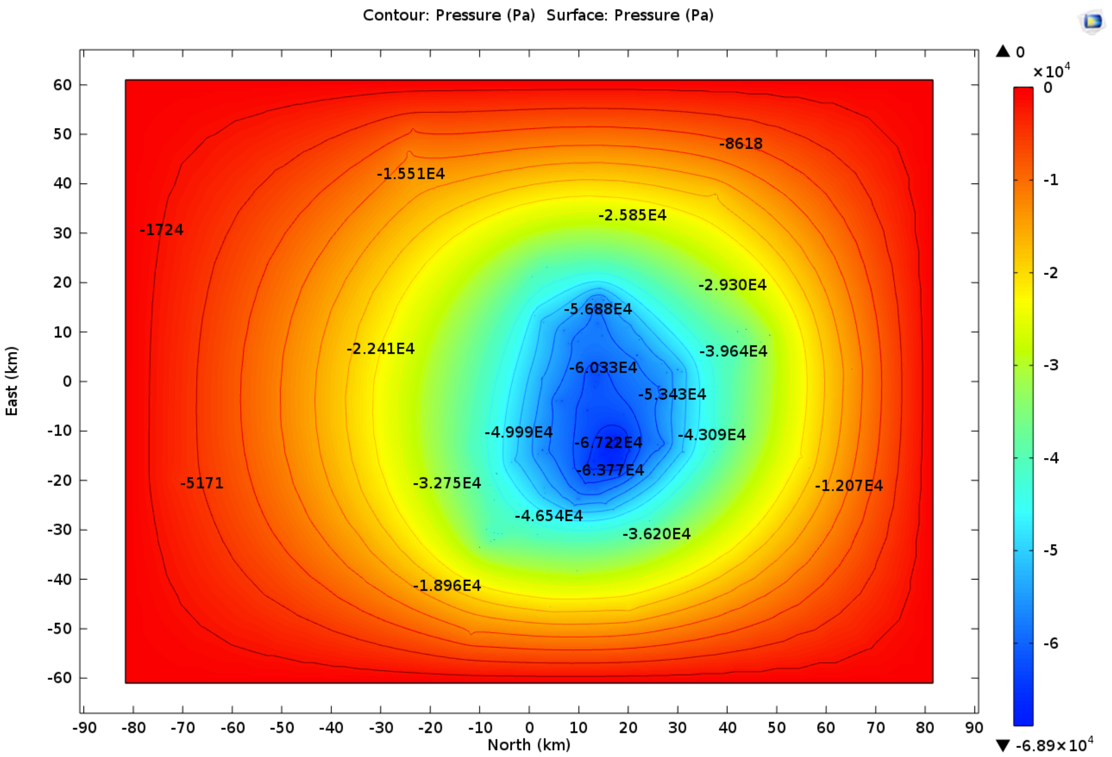

Figure 19 Pressure Distribution for Typical Sand

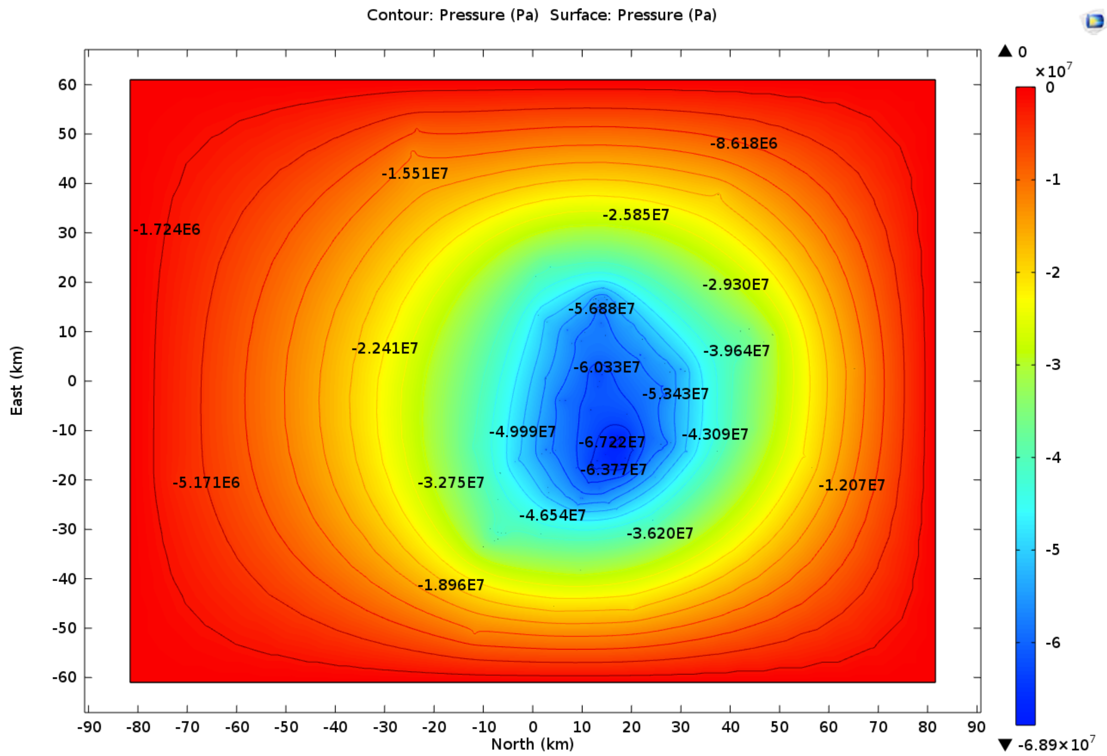

Figure 20 Pressure Distribution for Typical Clay

The second step is to analyse the effect of the variation in zero-pressure boundary on pressure distribution. The peak pressure reductions in sandy aquifer with different distance between the boundary and the furthest boreholes are shown in Table 2. From this table, increases in sizes of boundaries cause increases in the peak pressures. However, as the increasing trend diminishes, and the increase in pressure is less than 10%, the effect of the increase in boundaries is limited and might not be significant.

3.4.2. Influence Zone

The influence zones represented by contours of water extraction are simulated as the temperature fields due to cold-water injection. The transformation procedure is explained in section 3.2.2. The rock properties, including permeability and porosity, are based on the sandstone. As shown from Figure 21 to Figure 24, the temperature fields are plotted after the extraction of hot water for 10, 50, 100 and 200 years. The legend is shown on the right of graph, the colour changes from red to blue illustrates the temperature changes from 70 ^{o}C to 20 ^{o}C. In each graph, the border of the red region is the border of influence zone, as the red colour means the aquifer temperature is not lower due the injected cold water. A combined influence zones at different time intervals is shown in Figure 25. This graph is coloured lines are the hot ground water contours at different time period, including 10, 50,100 and 200 years. As the time period increases from 10 to 200 years, the influence zone increases accordingly. At 5 years, the influence zone is limited to the surrounding area of the wells. As the wells are concentrated at centre of Beijing, the effect is limited within this region as well. At 50 years, the influence zone is a circular shape and the furthest wells locate at the perimeter of the circle. The effect is limited to urban area of Beijing. At 100 years, the influence zone nearly expands to the boundaries of simulated region. This means that the hot water resources in Beijing can sustain the extraction rates for 100 years. After 100 years, the influence zone will outspread into adjacent cities as shown by the contour at 200 years.

This analysis bases on a transformation from the temperature field to fluid field with carefully chosen parameters based on the physical meaning. The temperature should ideally be exactly between 20 ^{o}C (temperature of the cold injection water) to 70 ^{o}C (average temperature of the hot underground water). However, the simulation result is 5 ^{o}C away. Possible reason is that this method is still an indirect simulation. The conversion between the fields inevitably causes oscillation.

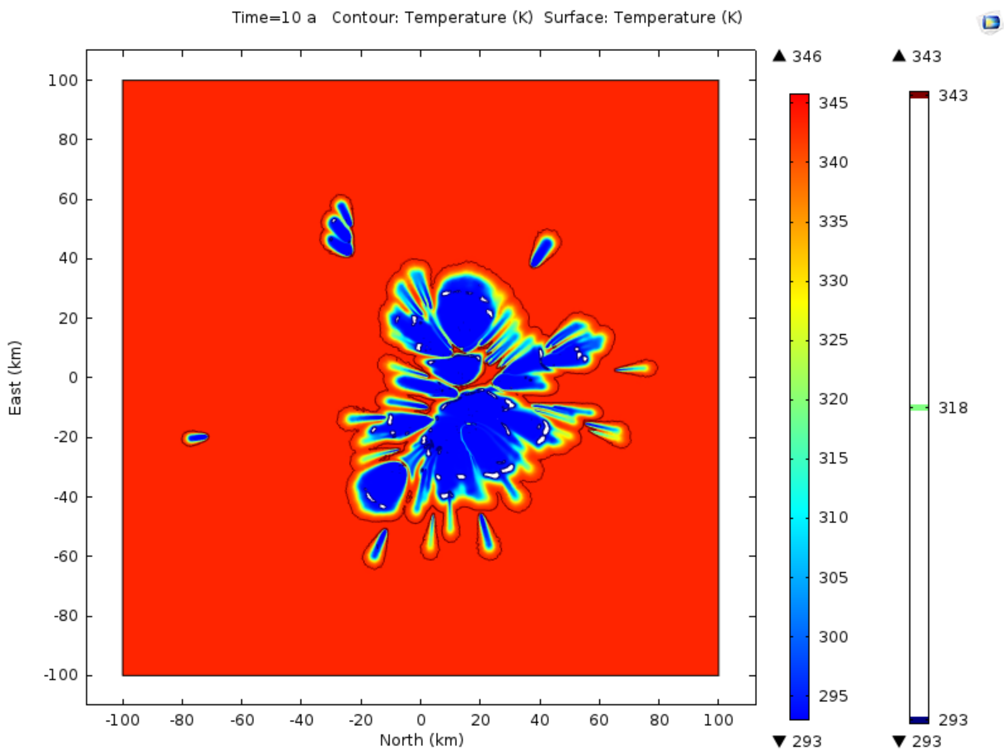

Figure 21 Temperature Field at 10 Years

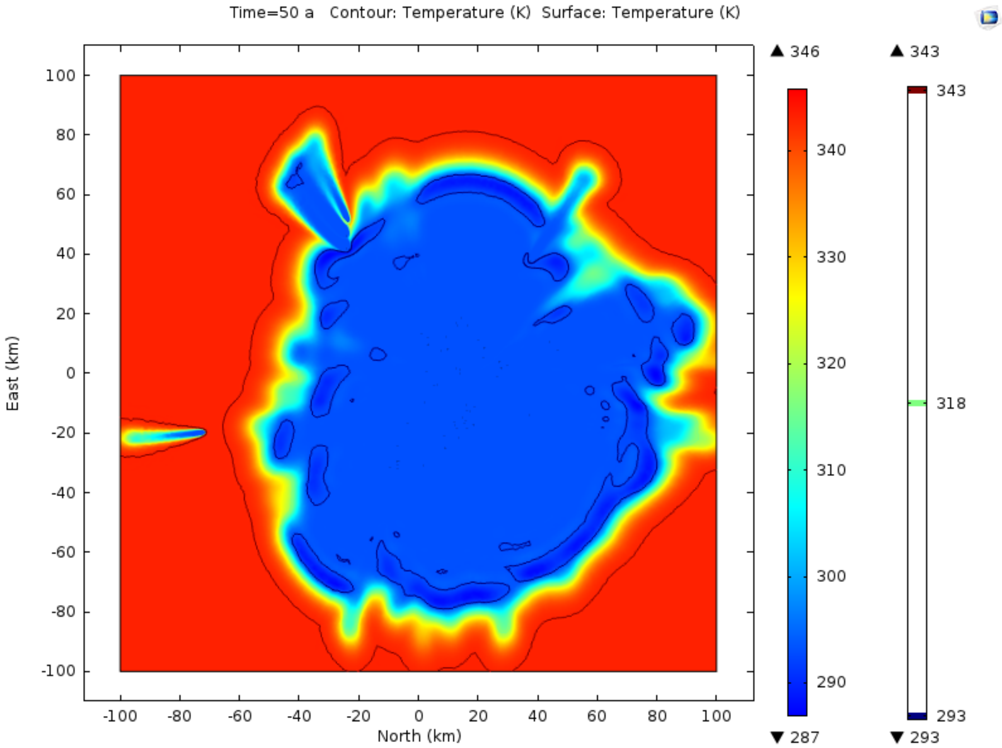

Figure 22 Temperature Field at 50 Years

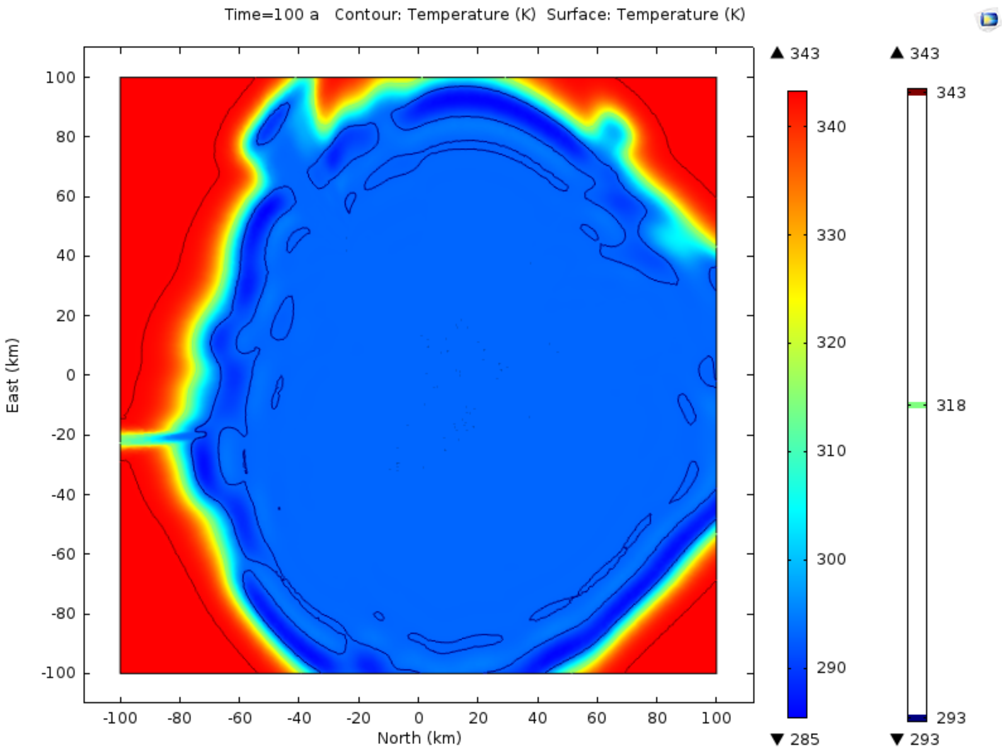

Figure 23 Temperature Field at 100 Years

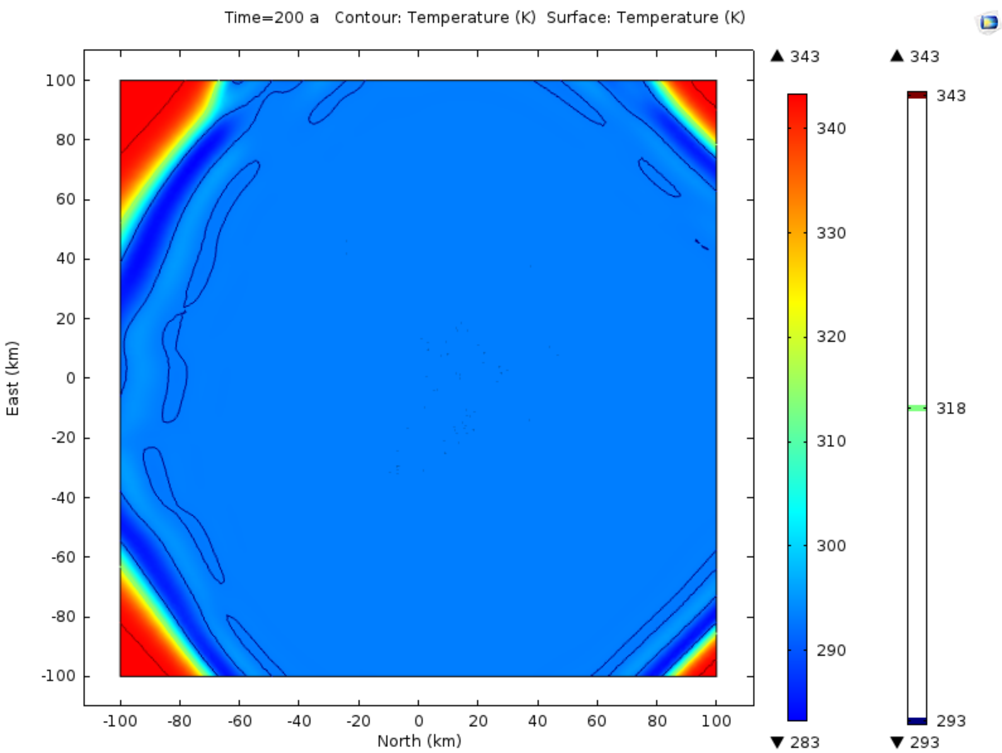

Figure 24 Temperature Field at 200 Years.

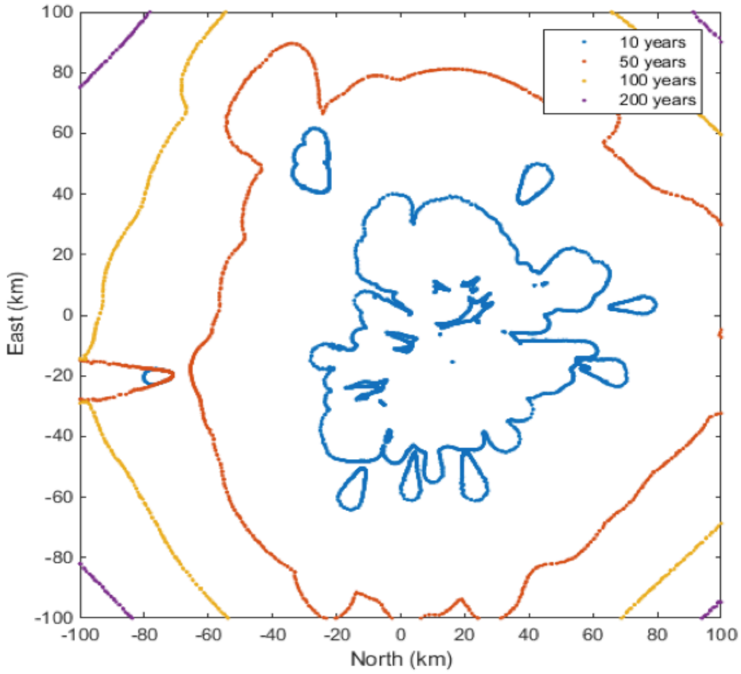

Figure 25 Water Contours at Different Time Intervals

4. Conclusion

A methodology was presented for assessing the geothermal potential in the subsurface in Beijing. Detailed statistics analysis was carried out. The distributions of well depths and temperature at the bottom of wells were obtained. Spatial relationship between the concentration of borehole data and degree of urbanization was verified. Correlation between temperature profile and depth of wells was conducted from best-fit line of the borehole data, and was also compared with theoretical correlation of general earth characteristics. Detailed 3D model for defining the geological information (horizons, and aquifers) and borehole data (well locations and depths) was combined with utilization scenarios.

FEA was carried out in 2D over the area. The equilibrium pressure distribution with the constant outflow rates was simulated based on Darcy's Law. The influences on pressure distribution with different soil types and different zero-pressure boundaries were quantified. The influence zones (the exhausted hot contours) were illustrated at different time periods.

From the statistical analysis, the well locations and temperature profiles for individual borehole is easily identified to carry out individual borehole analysis. At the same time, for city-scale planning, average temperature at particular depth can be calculated from the correlation. From the 3D geological map, wells located in each aquifer is identified and selected to carry out detailed FEA. Aquifer thickness at any point within the area is extracted from the geological model in order to analyse the effect of extracting hot water in volumetric method.

FEA in 2D provides a simplified solution for the pumping systems and sustainability study. The simplified solution is valid with carefully calibrated outflow rates and boundary conditions. Pressure required at any points in the region can be extrapolated and then provided as a guideline for pumping design. The sustainability of the geothermal energy can be indicated by the size of the influence zone, i.e. number of years that hot ground water could maintain the current extraction rates before exhaustion.

The 3D geological map can be future input into numerical analysing tool to evaluate the geothermal potential. The heat extracted from the region can be calculated with energy equation. The 2D FEA results can be combined with aquifer thickness information to produce a 3D FEA. As there are 600 existing extractions, the current borehole allocations can be multiplied in order to assess the full potential. The quality of geological model can be improved by either acquiring new geological data or obtaining the seismic and fault data. As the seismic and fault data can have a significant effect on the permeability of the soil, and hence the pressure distribution over the area.

5. Reference

[1] I. B. Fridleifsson, “Geothermal energy for the benefit of the people,” Renew. Sustain. Energy Rev., vol. 5, no. 3, pp. 299–312, Sep. 2001.

[2] E. Barbier, “Geothermal energy technology and current status: an overview,” Renew. Sustain. Energy Rev., vol. 6, no. 1–2, pp. 3–65, Jan. 2002.

[3] S. Haehnlein, P. Bayer, and P. Blum, “International legal status of the use of shallow geothermal energy,” Renew. Sustain. Energy Rev., vol. 14, no. 9, pp. 2611–2625, Dec. 2010.

[4] D. Giardini, “Geothermal quake risks must be faced.,” Nature, vol. 462, no. 7275, pp. 848–849, 2009.

[5] C. Energy and T. Flagship, “CSIRO ENERGY TRANSFORMED FLAGSHIP AEMO 100 % Renewable Energy Study,” 2012.

[6] T. Kujawa, W. Nowak, and A. a. Stachel, “Utilization of existing deep geological wells for acquisitions of geothermal energy,” Energy, vol. 31, no. 5, pp. 650–664, 2006.

[7] X. G. Zhao and G. Wan, “Current situation and prospect of China’s geothermal resources,” Renew. Sustain. Energy Rev., vol. 32, pp. 651–661, 2014.

[8] Y. Qilong, G. Bodvarsson, and G. Axelsson, “Geothermal resources of the Beijing area, China,” Geothermics, vol. 15, no. 2, pp. 157–166, 1986.

[9] G. Axelsson, Á. Gudmundsson, B. Steingrímsson, G. Pálmason, H. Ármannsson, H. Tulinus, Ó. G. Flóvenz, S. Björnsson, and V. Stefánsson, “Sustainable production of geothermal energy: suggested definition,” IGA-News, vol. 53. pp. 1–2, 2001.

[10] G. Axelsson and V. Stefánsson, “Sustainable management of geothermal resources,” Int. Geotherm. Conf. Reykjavík, pp. 40–48, 2003.

[11] C. Wijns, F. Boschetti, and L. Moresi, “Inverse modelling in geology by interactive evolutionary computation,” J. Struct. Geol., vol. 25, no. 10, pp. 1615–1621, 2003.

[12] Q. Wu, H. Xu, and X. Zou, “An effective method for 3D geological modeling with multi-source data integration,” Comput. Geosci., vol. 31, no. 1, pp. 35–43, 2005.

[13] P. Calcagno, C. Baujard, L. Guillou-Frottier, a. Dagallier, and a. Genter, "Estimation of the deep geothermal potential within the Tertiary Limagne basin (French Massif Central): An integrated 3D geological and thermal approach," Geothermics, vol. 51, pp. 496–508, 2014.

[14] A. Genter, L. Guillou-Frottier, J. L. Feybesse, N. Nicol, C. Dezayes, and S. Schwartz, "Typology of potential Hot Fractured Rock resources in Europe," Geothermics, vol. 32, no. 4, pp. 701–710, 2003.

[15] A. Genter, K. Evans, N. Cuenot, D. Fritsch, and B. Sanjuan, "Contribution of the exploration of deep crystalline fractured reservoir of Soultz to the knowledge of enhanced geothermal systems (EGS)," Comptes Rendus - Geosci., vol. 342, no. 7–8, pp. 502 – 516, 2010.

[16] R. Millot, P. Négrel, and E. Petelet-Giraud, "Multi-isotopic (Li, B, Sr, Nd) approach for geothermal reservoir characterization in the Limagne Basin (Massif Central, France)," Appl. Geochemistry, vol. 22, no. 11, pp. 2307–2325, 2007.

[17] P. Calcagno, V. Bouchot, I. Thinon, and B. Bourgine, "A new 3D fault model of the Bouillante geothermal province combining onshore and offshore structural knowledge (French West Indies)," Tectonophysics, vol. 526–529, pp. 185–195, 2012.

[18] Y. Teng and K. Koike, "Three-dimensional imaging of a geothermal system using temperature and geological models derived from a well-log dataset," Geothermics, vol. 36, no. 6, pp. 518–538, 2007.

[19] T. Kohl, N. Andenmatten, and L. Rybach, "Geothermal resource mapping-example from northern Switzerland," Geothermics, vol. 32, no. 4, pp. 721–732, 2003.

[20] J.-L. Mallet, "Discrete smooth interpolation," ACM Trans. Graph., vol. 8, no. 2, pp. 121–144, 1989.

[21] T. Kohl, K. F. Evansi, R. J. Hopkirk, and L. Rybach, "Coupled hydraulic, thermal and mechanical considerations for the simulation of hot dry rock reservoirs," Geothermics, vol. 24, no. 3, pp. 345–359, 1995.

[22] R. B. Xiao, Q. H. Weng, Z. Y. Ouyang, W. F. Li, E. W. Schienke, and Z. M. Zhang, "Land surface temperature variation and major factors in Beijing, China," Photogramm. Eng. Remote Sensing, vol. 74, no. 4, pp. 451–461, 2008.

Appendix 1

Risk Assessment Retrospective:

The initial risk assessment form neglected the severity of the risks involved, as the risk of computational task is thought to be low. The impact of risks due to the workspace and posture is not fully evaluated. This research's major challenge is to analysis the massive amount of borehole data, which indicate large amount of repetitive motions in more than five hours. The severances of the poor workspace and poor posture would have an exponential effect to the body condition. Tripping hazards are also likely to occur both in the workspace and the path access to the workspace. Intensive use of eyes over the time period caused exhaust eyes and lower immunity. As a result, sicknesses like stye and myopia occurred. Discomfort and low productivity occurred due to glare and insufficient lighting. The main workspace is located in the basement; productivity was further lowered due to insufficient ventilation, air freshness, and odors from the neighboring machines. In retrospective, a more practical and thorough risk assessment should have been produced through the use of designated workspace and a guideline for posture. The risk assessment should include all the risk assessments, including their likelihood of occurrence, impact and corresponding emergent and long-term remedial actions. In the cases where the impact is subtle, the productivity and comfort should be quantified, where are related to the project progress.

Appendix 2-Tables:

Table 1: Outlet Velocity, well locations inputted in COMSOL

Well name	x (km)	y (km)	Rate(m^3/day)	Outflow(m/s)
Jingre-34	20.34	-14.05	1488.00	0.0055
Jingre-5	14.66	-14.78	1.9cm3/s	0.0061
Tuan-5	18.61	-10.40	668m3/h	0.0061
Jingre-57	17.22	-12.77	1506.00	0.0056
	24.74	-19.50	1500.00	0.0055
JIngre-54	8.54	-20.67	1337.00	0.0049
Jingre-49	55.16	-15.27	1240.00	0.0046
Jingre-50	15.85	-12.46	780.00	0.0029
Jingre-45	11.57	-19.58	1020.00	0.0038
Jingre-40	12.16	-17.37	1054.00	0.0039
Ren-2	16.04	-12.75	1144.00	0.0042
Jingre-55	18.50	-13.55	1528.00	0.0056
Jingre-51	56.43	-17.55	542.00	0.0020
Jingre-44	12.93	-18.41	392.00	0.0014
Jingre-48	15.73	-15.91	6.98	0.0022
Ding1-5	25.95	-12.70	1420.00	0.0052
Jingre-59	3.11	-22.64	1550.00	0.0057
Jingre-85	13.48	-21.71	23.21dm3/s	0.0074
Jingre-66	17.75	-11.91	2383.00	0.0088
Jingre-15	65.24	2.59	9.38dm3/s	0.0030
Tongre-1	24.27	-28.19	2473.00	0.0091
LK-1	15.07	16.51	1550.00	0.0057
Tangre-24	12.85	-17.82	1002.00	0.0037
Jingre130	13.21	-1.06	1506.00	0.0056
Jingre133	11.81	-22.11	1348.00	0.0050
Jingre134	11.27	-20.52	1708.00	0.0063
Jingre136	19.01	-11.43	12.5cm3/s	0.0040
Jingre137	18.04	-18.73	1212.00	0.0045
Jingre138	16.61	-16.56	2163.00	0.0080
Jingre-142	16.42	-18.30	1337.00	0.0049

Jingre-139	1.81	-14.76	1878.00	0.0069
Jingre-144	18.66	-15.64	2163.00	0.0080
Jingre-120	18.97	-6.62	1019.00	0.0038
Jingre-148	11.96	-17.01	1549.00	0.0057
Jingre-151	3.61	-14.60	518.00	0.0019
Jingre-157	16.01	-10.66	1028.00	0.0038
Jingre-149	2.67	0.49	1272.00	0.0047
Yuanre-2	14.10	1.35	2409.00	0.0089
Jingre-132	9.12	-25.04	2148.00	0.0079
Tangre-33	13.26	16.26	1090.00	0.0040
Tangre-14	1.19	13.38	1441.00	0.0053
Xin001	12.70	16.65	507.00	0.0019
Tangre-29	13.40	14.02	1506.00	0.0056
Tangre-16	14.33	11.22	1089.00	0.0040
Suire-11	41.85	5.77	1036.00	0.0038
Share-5	7.95	7.69	887.00	0.0033
Suire-12	41.69	5.13	2592.00	0.0096
Xingre-3#	17.03	-25.92	902.00	0.0033
Share-9#	9.92	8.12	2163.00	0.0080
Changre-2#	2.07	24.10	1378.00	0.0051
Tongre-3#	44.51	-9.64	1482.00	0.0055
Shareguan-01	13.66	11.72	1665.00	0.0061
Share-10	13.17	2.90	1143.00	0.0042
Share-1#	12.78	1.88	4008.00	0.0148
Shuangre-1#	27.96	-12.41	1431.00	0.0053
Share-3	9.04	12.24	1019.00	0.0038
Tongre-4	31.21	-14.27	2083.00	0.0077
Shunhoure-2#	22.74	4.64	1328.00	0.0049
Tongre-5#	37.95	-10.80	935.00	0.0034
Share-012	6.99	10.30	3237.00	0.0119
Changre-04	0.74	19.69	1054.00	0.0039
Tongre-6#	33.92	-14.86	1002.00	0.0037
Share-11#	2.99	12.06	3413.00	0.0126
Xingre-04#	4.27	-45.60	776.00	0.0029
Tongre-8	37.41	-14.15	825.00	0.0030

Yanre-4	-24.29	46.30	3068.00	0.0113
Yongre-1	-11.74	-51.00	1991.00	0.0073
Xingre-6	1.69	-30.96	1979.00	0.0073
Shunhoure-6	21.81	5.33	1328.00	0.0049
Shunhoure-5	20.02	11.07	2400.00	0.0088
Jingre-167	-3.57	-16.34	1856.00	0.0068
Shunre006	25.69	3.33	530.00	0.0020
Jingre-146	13.58	-0.03	1317.60	0.0049
Changre007	3.59	23.10	1726.00	0.0064
Jingre119	5.42	-3.93	2232.00	0.0082
Jingre132	10.06	-23.75	2148.25	0.0079
Jingre139	2.65	-13.85	2148.25	0.0079
Jingre142	17.28	-17.14	1337.00	0.0049
Jingre148	13.06	-16.11	1549.70	0.0057
Jingre150	9.67	-23.68	1978.00	0.0073
Jingre151	4.58	-13.96	603.42	0.0022
Jingre153	2.42	-9.92	2163.80	0.0080
Jingre161	4.29	-27.04	1089.59	0.0040
Jingre162	26.96	-2.82	1229.82	0.0045
Jingre167	-2.55	-15.74	1804.81	0.0067
Jingre168	6.55	-3.99	2555.70	0.0094
Jingreguan8	15.36	-16.94	1965.17	0.0072
Share15	3.20	9.60	1144.00	0.0042
Shunhoure6	48.59	9.38	1840.00	0.0068
Shunhoure8	22.19	8.54	1369.00	0.0050
Shunre6	27.10	3.99	530.00	0.0020
Shunre7	26.80	3.58	810.00	0.0030
Shunre8	24.42	-11.64	810.00	0.0030
Shunreguan1	30.78	1.96	2110.70	0.0078
Suire14	40.89	5.55	1484.00	0.0055
Suire15	26.31	-0.99	1308.00	0.0048
Tangre62	14.77	9.17	1054.00	0.0039
Tangre68	0.70	21.10	1781.00	0.0066
Tongre10	37.44	-9.35	1389.00	0.0051
Yanre2guan	-23.83	41.96	2832.00	0.0104

Yongre1	-11.63	-13.23	1991.00	0.0073
Jingre-65	13.90	-22.39	1200.00	0.0044
D-3	37.64	37.68	2905.00	0.0107
Jingre56#	18.53	-17.32	2592.00	0.0096
Jingre-63	16.21	-12.76	1328.00	0.0049
Jingre-64	26.80	-12.70	16.68L/s	0.0053
Jingre-61	26.83	-12.28	1337.00	0.0049
Jingre62#	-71.59	-19.68	1133.00	0.0042
Jingre72#	16.75	-13.05	1337.00	0.0049
Jingre73#	-7.11	-24.01	1034.00	0.0038
Jingre-67	8.83	-17.55	1108.00	0.0041
Jingre69#	17.25	-11.20	1594.00	0.0059
Jingre70	15.38	-24.61	2308.00	0.0085
Jingre-71	9.66	-38.22	1099.00	0.0041
Jingre83	18.43	-16.97	2308.00	0.0085
Jingre78	27.30	-12.66	1239.00	0.0046
Jingre80	24.65	-1.86	2016.00	0.0074
Jingre74	26.07	-13.76	1200.00	0.0044
Jingre92	-6.61	-18.65	1338.00	0.0049
Jingre81	11.73	-5.85	2031.00	0.0075
Jingre75	6.79	-23.18	1050.00	0.0039
Jingre77	11.87	-16.51	1002.00	0.0037
Tangre21	12.89	16.84	810.00	0.0030
Tangre-36	13.64	17.02	1011.00	0.0037
Tangre88L	3.10	-21.48	16.68 L/s	0.0053
Tangre39	12.25	16.33	1780.00	0.0066
Tangre34	14.60	17.04	1108.00	0.0041
Tangre-31	15.00	16.39	1550.00	0.0057
Tangre45	13.86	13.73	2059.00	0.0076
Tangre46	19.02	15.00	1109.00	0.0041
Tangre44	14.24	18.75	1337.00	0.0049
Tangre43	13.95	16.76	1338.00	0.0049
Tangre48	13.21	14.60	2444.00	0.0090
Tangre53	16.71	16.00	1338.00	0.0049
Tangre56	13.05	16.99	749.00	0.0028

Tangre63	14.81	16.98	1506.00	0.0056
Tangre698	13.91	11.69	1781.00	0.0066
Liangre1	-7.01	-31.89	154.00	0.0006
	-8.24	-32.36	1144.00	0.0042
Bian001	-7.81	-32.36	1600.00	0.0059
B1	-6.80	-30.93	2163.00	0.0080
B2	-6.97	-30.47	1278.00	0.0047
B3	-6.39	-30.72	1250.00	0.0046
Liangre015	-9.93	-33.63	1550.00	0.0057
Liangre017	-7.01	-29.43	840.00	0.0031
Liangre025	-9.60	-31.67	969.00	0.0036
Liangre024	-8.46	-31.66	1128.00	0.0042
Liangre026	-8.63	-30.05	2031.00	0.0075
Liangre030	-6.64	-29.60	1249.00	0.0046
Liangre028	-5.54	-30.77	1163.00	0.0043
XinYanre1	-23.49	51.00	1829.00	0.0067
Zhure008	42.00	10.09	1780.00	0.0066
Zhure005	43.85	10.55	1337.00	0.0049
Shunre1	30.01	2.39	2905.00	0.0107
Shunre002	27.79	1.88	1550.00	0.0057
Zhu-9	46.83	7.84	1954.00	0.0072
Xingre-2	20.14	-45.73	2031.00	0.0075
Zhu-10	44.07	8.56	1662.00	0.0061
Share7	10.61	9.75	840.00	0.0031
Share8＃	2.06	14.82	1219.00	0.0045

Appendix 3-Codes:

Code 1:

```
startP = 1; % startP*delta is the depth starting to calculate temperature
endP = 40; %the number of temperatures to be calculated from the fitted function
polynomial = 2; % set the degree of polynomial
delta = 100; % scale division for depth/m

[a,b] = size(oriData);
n = a/2; % number of data sets
clear temCal;
m = endP-startP+1;
temCal = zeros(2*n,m);

for i = 1:n;
    temCal((2*i-1),:) = delta*(startP:endP); % the depth for calculated temperature

    dep = nonzeros(oriData(2*i-1,:)); % depth obtained from the original data
    temp = nonzeros(oriData(2*i,:)); % temperature obtained from the original data
    temCal(2*i,:) = tFit2(dep,temp,m,temCal(1,:),polynomial);

    figure;
    plot(dep,temp,'b*-'); %plot orginal data
    hold on;
    plot(temCal((2*i-1),:),temCal((2*i),:),'ro');
    title(num2str(i));
    legend('orginal data','fitted data','location','northwest');
end;

%clear a b co delta i m n dep temp;
```

Code 2:

```
clc;
clear a b count d fn0 h H i j ln0 n t sizH theoT theoH tempIndex tempRecord tempAver;
```

```
% parameters
H = [500,1000,1500,2000,2500,3000,3500,4000];% selected depths
dH = 1000;
dT = 5;% temperature deviating from theoretical value
groundT = 15;% ground temperature
theoH =0:dH:3000;
n = 0;

%record the indexes of required depths
d = size(depth);
h = size(H);
for i = 1:d(2)
    for j = 1:h(2)
        if depth(1,i) == H(1,j)
            count(n+1) = i;
            n = n+1;
        end
    end
end
clear i j;

% plot temperature vs. depth
% record temperature at each depth
[a b]=size(temp);
tempIndex = ones(1,d(2));
for i = 1:a
    fn0 = 0;
    ln0 = 0;
    for j = 1:n
        t(i,j) = temp(i,count(j));
        h(i,j) = depth(count(j));
        if t(i,j) > 0
            ln0 = j;
            if fn0 == 0
                fn0 = j;
```

```
        end
      end
    end
    if fn0 > 0;
      plot(t(i,fn0:ln0),-h(i,fn0:ln0),'.b');
      hold on;

      for k = fn0:ln0;
        tempRecord((h(i,k)/500),tempIndex(h(i,k)/500)) = t(i,k);
        tempIndex(h(i,k)/500) = tempIndex(h(i,k)/500)+1;
      end
    end
end
clear i j;
hold on;

% calculate average temperature for each depth
tempAver = zeros(1,d(2));
rs = size(tempRecord);
for i = 1:rs(1);
    num = tempIndex(i)-1;
    tempAver(i) = sum(tempRecord(i,:))/num;

    %plot(tempAver(i),-500*i,'o');
    %hold on;
end
clear num;

% polyfit the average temperature vs depth
p=polyfit(tempAver(1:rs(1)),-500*(1:rs(1)),1);
x =0:100;% temperature axis
y = polyval(p,x);% depth axis
plot(x,y,'--');
hold on;
```

```
sizeH = size(theoH);
for i = 1:sizeH(2)
   theoT(i) = 30/1000*theoH(i)+groundT;
end
%plot theoretical lines
plot(theoT,-theoH,'r');
hold on;
plot(theoT+dT,-theoH,'g',theoT-dT,-theoH,'g');

xlabel('Temperature / °Ê');
ylabel('Depth / m');
axis([0,100,-4000,0]);

hold off;
```